

**NOAA NESDIS**  
**CENTER for SATELLITE APPLICATIONS and**  
**RESEARCH**

**GOES-R Advanced Baseline Imager  
(ABI) Algorithm Theoretical Basis  
Document  
For  
SO<sub>2</sub> Detection**

*Michael Pavolonis, NOAA/NESDIS/STAR  
Andrew Parker, UW-Madison SSEC/CIMSS*

Version 1.0  
September 15, 2010

## TABLE OF CONTENTS

|  |    |
|--|----|
| LIST OF ACRONYMS .....                                 | 5  |
| 1 Introduction.....                                    | 7  |
| 1.1 Purpose of This Document.....                      | 7  |
| 1.2 Who Should Use This Document .....                 | 7  |
| 1.3 Inside Each Section.....                           | 7  |
| 1.4 Related Documents .....                            | 7  |
| 1.5 Revision History .....                             | 8  |
| 2 OBSERVING SYSTEM OVERVIEW.....                       | 9  |
| 2.1 Products Generated .....                           | 9  |
| 2.1.1 Product Requirements.....                        | 9  |
| 2.2 Instrument Characteristics .....                   | 10 |
| 3 ALGORITHM DESCRIPTION.....                           | 11 |
| 3.1 Algorithm Overview .....                           | 11 |
| 3.2 Processing Outline .....                           | 11 |
| 3.3 Algorithm Input .....                              | 13 |
| 3.3.1 Primary Sensor Data .....                        | 13 |
| 3.3.2 Ancillary Data.....                              | 13 |
| 3.3.3 Radiative Transfer Models.....                   | 13 |
| 3.4 Theoretical Description.....                       | 14 |
| 3.4.1 Physics of the Problem.....                      | 14 |
| 3.4.2 Mathematical Description.....                    | 24 |
| 3.4.3 Algorithm Output.....                            | 32 |
| 4 TEST DATA SETS AND OUTPUTS.....                      | 33 |
| 4.1 Simulated/Proxy Input Data Sets .....              | 33 |
| 4.1.1 SEVIRI Data .....                                | 34 |
| 4.1.2 MODIS Data .....                                 | 35 |
| 4.2 Output from Simulated/Proxy Inputs Data Sets.....  | 37 |
| 4.2.1 Precisions and Accuracy Estimates .....          | 39 |
| 4.2.2 Error Budget.....                                | 40 |
| 5 PRACTICAL CONSIDERATIONS.....                        | 41 |
| 5.1 Numerical Computation Considerations.....          | 41 |
| 5.2 Programming and Procedural Considerations .....    | 41 |
| 5.3 Quality Assessment and Diagnostics .....           | 41 |
| 5.4 Exception Handling .....                           | 41 |
| 5.5 Algorithm Validation .....                         | 41 |
| 6 ASSUMPTIONS AND LIMITATIONS .....                    | 42 |
| 6.1 Performance .....                                  | 42 |
| 6.2 Assumed Sensor Performance .....                   | 43 |
| 6.3 Pre-Planned Product Improvements .....             | 43 |
| 6.3.1 Incorporation of second water vapor channel..... | 43 |
| 7 REFERENCES .....                                     | 44 |

## LIST OF FIGURES

|   |    |
|---|----|
| Figure 1: High Level Flowchart of the ABI_SO2 illustrating the main processing sections.....  | 12 |
| Figure 2: Simulated brightness temperature difference between a 1 Dobson Unit (DU) loading of SO <sub>2</sub> and a 550 DU loading as a function of wavelength. The ABI spectral bandwidths for channel 10 (7.4 $\mu\text{m}$ ) and channel 11 (8.5 $\mu\text{m}$ ) are shaded in gray. Wavelengths longer than about 9 $\mu\text{m}$ are not shown since the impact of SO <sub>2</sub> is minimal at those wavelengths. In the infrared, only ABI channels 10 and 11 are significantly impacted by SO <sub>2</sub> absorption..... | 15 |
| Figure 3: A false color SEVIRI image (September 30, 2007, 1500 UTC) indicating the location of the ice, liquid water, dust, and SO <sub>2</sub> clouds selected to illustrate the multi-spectral microphysical signal exhibited by different cloud type. ....   | 21 |
| Figure 4: The 2D distribution of $\beta_{\text{stropo}}(8.5/11\mu\text{m})$ and $\beta_{\text{stropo}}(12/11\mu\text{m})$ for 4 different cloud types (ice, liquid water, dust, and SO <sub>2</sub> ) observed by SEVIRI on September 30, 2007 at 1500 UTC.....   | 22 |
| Figure 5: The 2D distribution of $\beta_{\text{stropo}}(8.5/11\mu\text{m})$ and $\beta_{\text{stropo}}(7.4/11\mu\text{m})$ for 4 different cloud types (ice, liquid water, dust, and SO <sub>2</sub> ) observed by SEVIRI on September 30, 2007 at 1500 UTC. The absence of liquid water and dust data points .....   | 22 |
| Figure 6: The normalized joint frequency of occurrence of $\beta_{\text{stropo}}(8.5/11\mu\text{m})$ and $\beta_{\text{stropo}}(12/11\mu\text{m})$ for three different $\epsilon_{\text{stropo}}(8.5 \mu\text{m})$ bins.....  | 26 |
| Figure 7: The normalized joint frequency of occurrence of $\beta_{\text{stropo}}(8.5/11\mu\text{m})$ and $\beta_{\text{stropo}}(7.4/11\mu\text{m})$ for three different $\epsilon_{\text{stropo}}(7.4 \mu\text{m})$ bins.....   | 27 |
| Figure 8: SEVIRI RGB image from 12 UTC on November 24, 2006. ....   | 35 |
| MODIS provides 36 spectral channels with a spatial resolution of 1 km and provides global coverage in low Earth orbit. MODIS has observed many volcanic eruptions. The MODIS to ABI channel mapping is shown in Table 9. An example MODIS false color image is shown in Figure 9. ....  | 35 |
| Figure 9: MODIS RGB image from 14 UTC on May 5, 2008. ....  | 36 |
| Figure 10: The OMI SO <sub>2</sub> loading product shows an SO <sub>2</sub> plume associated with an eruption of Jebel al-Tair in Yemen on October 1, 2007. ....  | 37 |
| Figure 11: Example results from the ABI-SO <sub>2</sub> are shown for a Met-8 SEVIRI observed eruption of Nyamuragira in central Africa on November 29, 2006 at 12:45 UTC. The full disk results are shown in the top row (false color on left, SO <sub>2</sub> detection in red on the right). A zoomed in view is shown in the bottom row, including an estimate of the SO <sub>2</sub> loading, which is stored in the quality flags. ....   | 38 |
| Figure 12: Example results from the ABI-SO <sub>2</sub> are shown for a <i>Aqua</i> -MODIS observed eruption of Kasatochi in the Aleutian Islands on August 11, 2008 at 22:05 UTC. The SO <sub>2</sub> detection results are overlaid as white contours on a false color image on the left panel and the estimated SO <sub>2</sub> loading is shown in the right panel.....   | 39 |
| Figure 13: The ABI SO <sub>2</sub> detection skill score is shown as a function of the OMI SO <sub>2</sub> loading in blue. The false alarm rate is shown in gray, and the required SO <sub>2</sub> detection skill score is shown in dashed red. The required detection skill score only applies to SO <sub>2</sub> loadings of 10 DU or greater. This analysis was constructed using over 270,000 data points.....  | 40 |

## LIST OF TABLES

|  |    |
|--|----|
| Table 1: GOES-R SO <sub>2</sub> Detection product requirements. The Geographic Coverage definitions are: M=Mesoscale, C=CONUS, and FD=Full Disk. ....  | 10 |
| Table 2: Channel numbers and wavelengths for the ABI. ....   | 10 |
| Table 3: Inputs used in calculation of Local Radiative Center (LRC). The gradient filter function used in the calculation is described in the AIADD document.....  | 23 |
| Table 4: The object statistics needed to filter out false alarm “beta objects.” The symbols used to denote the individual statistics is shown in bold in the first column.....   | 29 |
| <b>Table 5: The object statistics needed to filter out false alarm “btd objects.” The symbols used to denote the individual statistics is shown in bold in the first column.</b>   |    |
| .....  | 30 |
| Table 6: The logical tests used to determine if a “beta object” is an SO <sub>2</sub> cloud are shown. If all five logical tests return “true,” then the object is deemed to be SO <sub>2</sub> ; otherwise it is filtered out.....  | 31 |
| <b>Table 7: The logical tests used to determine if a “btd object” is an SO<sub>2</sub> cloud are shown. If all four logical tests return “true,” then the object is deemed to be SO<sub>2</sub>; otherwise it is filtered out.</b>   |    |
| .....  | 32 |
| Table 8: SO <sub>2</sub> Detection Quality Flag (QF) description. The Ash Detection QF Flags are bit packed byte variables. The byte column identifies the byte number(s) the QF is stored in and the Bit column lists the bit(s) the flag encompasses within the byte(s). The name of the each flag is included, along with possible values; the bold values are the initialized values. .... | 32 |
| Table 9: SO <sub>2</sub> detection PQI Flag description. The SO <sub>2</sub> detection PQI Flags are bit packed byte variables. The byte column identifies the byte number(s) the PQI is stored in and the Bit column lists the bit(s) the flag encompasses within the byte(s). The name of the each flag is included, along with possible values. ....  | 33 |
| Table 10: A description of the SO <sub>2</sub> detection metadata.....   | 33 |
| <b>Table 11: The SEVIRI bands used to test the ABI SO<sub>2</sub> detection algorithm is shown relative to the corresponding ABI bands.</b>  |    |
| .....  | 34 |
| Table 12: The MODIS bands used to test the ABI volcanic ash algorithm is shown relative to the corresponding ABI bands. ....   | 36 |

## **LIST OF ACRONYMS**

ABI – Advanced Baseline Imager  
ABI-VAA – Advanced Baseline Imager Volcanic Ash Algorithm  
AC – Above Cloud  
AIADD – Algorithm Interface and Ancillary Data Description  
ATBD – Algorithm Theoretical Basis Document  
AWG – Algorithm Working Group  
CDF – Cumulative Distribution Function  
CONUS – Continental United States  
DU – Dobson Units  
ECMWF – European Centre for Medium-Range Weather Forecasts  
EOS – Earth Observing System  
ESA – European Space Agency  
F&PS – Functional & Performance Specification  
GOES – Geostationary Operational Environmental Satellite  
LRC – Local Radiative Center  
MODIS – Moderate Resolution Imaging Spectroradiometer  
NASA – National Aeronautics and Space Agency  
NESDIS – National Environmental Satellite, Data, and Information Service  
NOAA – National Oceanic and Atmospheric Administration  
NWP – Numerical Weather Prediction  
OMI – Ozone Monitoring Instrument  
POES – Polar Operational Environmental Satellite  
SEVIRI – Spinning Enhanced Visible and Infrared Imager  
SSEC – Space Science and Engineering Center  
STAR – Center for Satellite Applications and Research  
TOA – Top of Atmosphere  
TRR – Test Readiness Review  
UTC – Coordinated Universal Time

## **ABSTRACT**

This document provides a high level description of the physical basis for the detection of sulfur dioxide ( $\text{SO}_2$ ) clouds within images taken by the Advanced Baseline Imager (ABI) flown on the GOES-R series of NOAA geostationary meteorological satellites. The ABI  $\text{SO}_2$  detection algorithm utilizes spectral and spatial information to determine if  $\text{SO}_2$  is present. The algorithm utilizes ABI channels 8 (6.2  $\mu\text{m}$ ) 10 (7.4  $\mu\text{m}$ ), 11 (8.5  $\mu\text{m}$ ), 14 (11  $\mu\text{m}$ ), and 15 (12  $\mu\text{m}$ ), which are all infrared channels. In lieu of brightness temperature differences, effective absorption optical depth ratios are used in the spectral tests. Effective absorption optical depth ratios, allow for improved sensitivity to the presence of  $\text{SO}_2$ , especially for optically thin clouds. In addition, a series of cloud object based filters are applied to greatly reduce false alarms. The validation analysis indicates that the algorithm will meet the accuracy requirements.

# 1 Introduction

## 1.1 Purpose of This Document

The SO<sub>2</sub> algorithm theoretical basis document (ATBD) provides a high level description of and the physical basis for the detection of SO<sub>2</sub> observed by the Advanced Baseline Imager (ABI) flown on the GOES-R series of NOAA geostationary meteorological satellites.

## 1.2 Who Should Use This Document

The intended user of this document are those interested in understanding the physical basis of the algorithms and how to use the output of this algorithm. This document also provides information useful to anyone maintaining or modifying the original algorithm.

## 1.3 Inside Each Section

This document is broken down into the following main sections.

- **System Overview:** Provides relevant details of the ABI and provides a brief description of the products generated by the algorithm.
- **Algorithm Description:** Provides all the detailed description of the algorithm including its physical basis, its input and its output.
- **Test Data Sets and Outputs:** Provides a detailed description of the data sets used to develop and test the GOES-R ABI algorithm and describes the algorithm output.
- **Practical Considerations:** Provides a description of algorithm programming and quality control considerations.
- **Assumptions and Limitations:** Provides an overview of the current limitations of the approach and gives the plan for overcoming these limitations with further algorithm development.

## 1.4 Related Documents

- GOES-R Functional & Performance Specification Document (F&PS)
- GOES-R ABI SO<sub>2</sub> Product Validation Plan Document
- Algorithm Interface and Ancillary Data Description (AIADD) Document

## **1.5 Revision History**

- 9/30/2009 - Version 0.1 of this document was created by Michael J Pavolonis (NOAA/NESDIS/STAR). Version 0.1 represents the first draft of this document.
- 7/31/2010 – Version 1.0 of this document was created by Michael J Pavolonis (NOAA/NESDIS/STAR). In this revision, Version 0.1 was revised to meet 80% delivery standards.
- 9/15/2010 – Version 1.0 of this document was revised by Michael J Pavolonis (NOAA/NESDIS/STAR). In this revision, Version 1.0 was revised based on reviewer comments.

## 2 OBSERVING SYSTEM OVERVIEW

This section will describe the products generated by the ABI SO<sub>2</sub> Detection Algorithm (ABI-SO<sub>2</sub>) and the requirements it places on the sensor.

### 2.1 Products Generated

The ABI-SO<sub>2</sub> is responsible for producing a SO<sub>2</sub> detection (yes/no) flag for all pixels. This includes pixels that contain SO<sub>2</sub> contaminated meteorological clouds. Actually, most SO<sub>2</sub> clouds also contain some ice/liquid water. This is verified by the fact that these clouds are visible in 11-μm imagery. A pure SO<sub>2</sub> gas cloud would not be visible in the 11-μm imagery.

#### 2.1.1 Product Requirements

The F&PS spatial, temporal, and accuracy requirements for the GOES-R SO<sub>2</sub> Detection product are shown below in Table 1.

| Name                      | User & Priority | Geographic Coverage | Vertical Res. | Horiz. Res. | Mapping Accuracy | Maint. Rang.  | Refresh Rate/Coverage Time Option (Mode 3) | Minmt. Accracy | Data Latency | Long-Term | Product Measurement Precision |                |
|---------------------------|-----------------|---------------------|---------------|-------------|------------------|---|--|----------------|--------------|-----------|-------------------------------|----------------|
| SO <sub>2</sub> Detection | GOES-R          | FD                  | Total Column  | 2 km        | 1 km             | Binary yes/no detection from 10 to 700 Dobson Units | 70% Correct Detection                      | 60 min         | 5 min        | 806 sec   | TBD                           | Not applicable |

| Name                      | User & Priority | Geographic Coverage | Temporal Coverage Qualifiers | Product Extend Qualifiers  | Cloud Cover Conditions Qualifiers                   | Product Statistics Qualifier   |
|---------------------------|-----------------|---------------------|------------------------------|--|---|--------------------------------|
| SO <sub>2</sub> Detection | GOES-R          | FD                  | Day and night                | Quantitative out to at least 70 degrees LZA and qualitative beyond | Clear conditions associated with threshold accuracy | Over specified geographic area |

**Table 1: GOES-R SO<sub>2</sub> Detection product requirements. The Geographic Coverage definitions are: M=Mesoscale, C=CONUS, and FD=Full Disk.**

## 2.2 Instrument Characteristics

Table 2 shows the ABI channels used in the SO<sub>2</sub> detection algorithm. The ABI-SO<sub>2</sub> relies on infrared measurements. Channels 10 (7.4  $\mu\text{m}$ ) and 11 (8.5  $\mu\text{m}$ ) both contain several SO<sub>2</sub> absorption lines. Channels 14 (11  $\mu\text{m}$ ) and 15 (12  $\mu\text{m}$ ) are not sensitive to SO<sub>2</sub>, but are sensitive to the presence of small hydrometeors, which are common in SO<sub>2</sub> contaminated clouds.

The performance of the SO<sub>2</sub> detection algorithm is sensitive to any imagery artifacts or instrument noise. Calibrated observations are also critical because the SO<sub>2</sub> algorithm compares the observed values to those from a forward radiative transfer model. The channel specifications are given in the F&PS section 3.4.2.1.4.0. We are assuming the performance outlined in the F&PS during our development efforts.

| Channel Number | Wavelength ( $\mu\text{m}$ ) | Used in ABI-SO2 |
|----------------|------------------------------|-----------------|
| 1              | 0.47                         |                 |
| 2              | 0.64                         |                 |
| 3              | 0.86                         |                 |
| 4              | 1.38                         |                 |
| 5              | 1.61                         |                 |
| 6              | 2.26                         |                 |
| 7              | 3.9                          |                 |
| 8              | 6.15                         | ✓               |
| 9              | 7.0                          |                 |
| 10             | 7.4                          | ✓               |
| 11             | 8.5                          | ✓               |
| 12             | 9.7                          |                 |
| 13             | 10.35                        |                 |
| 14             | 11.2                         | ✓               |
| 15             | 12.3                         | ✓               |
| 16             | 13.3                         |                 |

**Table 2: Channel numbers and wavelengths for the ABI.**

## **3 ALGORITHM DESCRIPTION**

Below is a complete description of the algorithm at the current level of maturity (which will improve with each revision).

### **3.1 Algorithm Overview**

Given the importance of monitoring SO<sub>2</sub> for aviation interests, health interests, and climate, the ABI-SO<sub>2</sub> serves an important role in the GOES-R ABI processing system. While a binary SO<sub>2</sub> detection flag is required, an estimate of the SO<sub>2</sub> loading is stored in the product quality flags.

The ABI-SO<sub>2</sub> derives the following product listed in the F&PS.

- SO<sub>2</sub> detection flag [yes/no]

In addition, the ABI-SO<sub>2</sub> derives the following products that are not included in the F&PS.

- Quality Flags (defined in Section)
- Product Quality Information (defined in Section)
- Metadata (defined in Section)

### **3.2 Processing Outline**

The processing outline of the ABI-SO<sub>2</sub> is summarized in the figure below. The ABI-SO<sub>2</sub> uses several spatial and spectral analysis routines. The ABI-SO<sub>2</sub> requires multiple scan lines of ABI data due to the spatial analysis that is utilized in the algorithm. Complete scan line segments should consist of at least the minimum number of scan lines required by the Gradient Filter, which is described in detail in the AIADD. While overlap between adjacent scan line segments is beneficial, scan line overlap was not used in the development and validation of this algorithm.

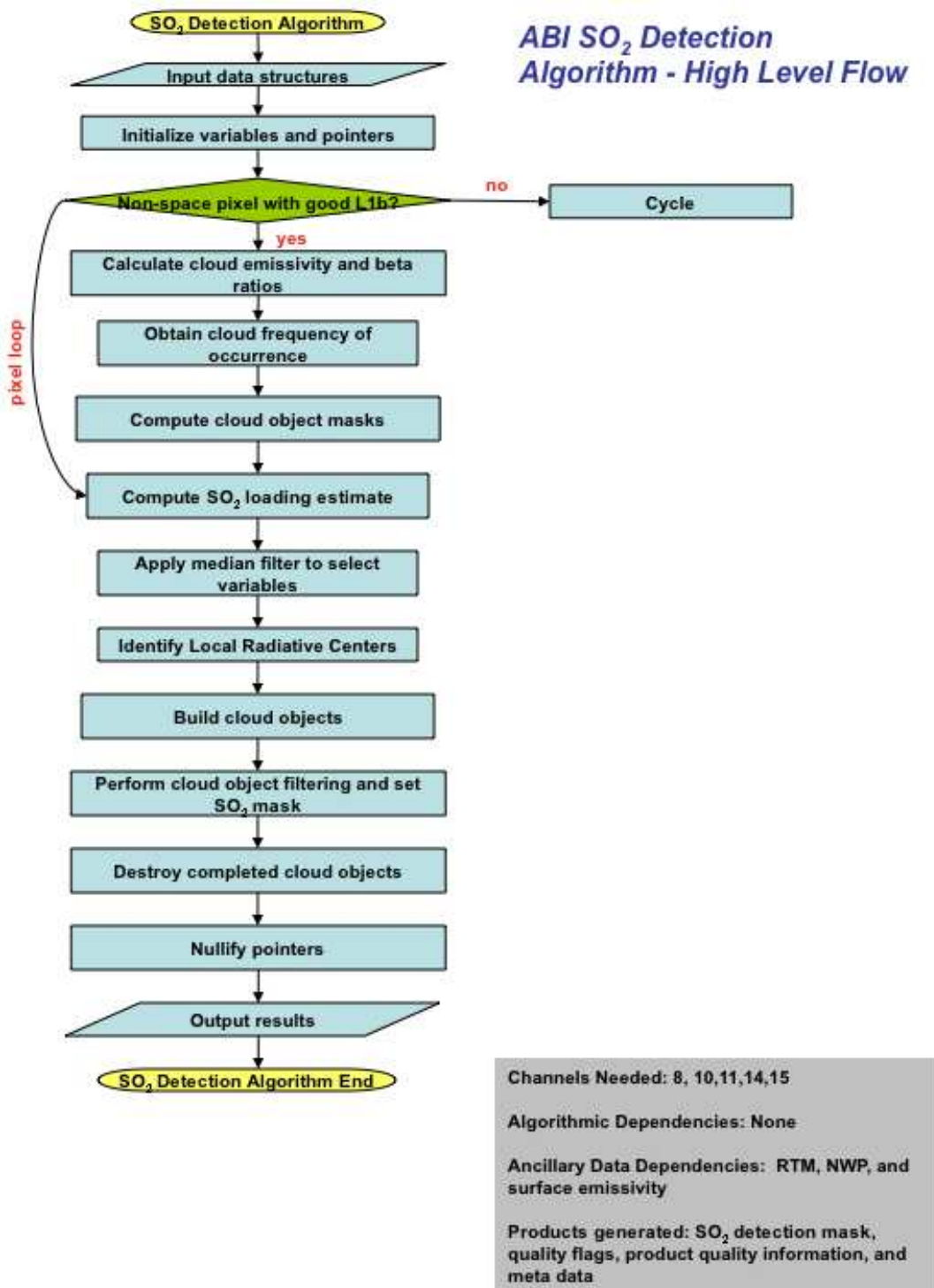


**Figure 1: High Level Flowchart of the ABI\_SO2 illustrating the main processing sections.**

### 3.3 Algorithm Input

This section describes the input needed to process the ABI-SO<sub>2</sub>. While the ABI-SO<sub>2</sub> operates on a pixel-by-pixel basis, surrounding pixels are needed for spatial analysis. Therefore, the ABI-SO<sub>2</sub> must have access to a group of pixels. In its current configuration, we run the ABI-SO<sub>2</sub> on segments comprised of 200 scan-lines. The minimum scan line segment size required to implement the ABI-SO<sub>2</sub> is driven by the minimum number of scan lines required to fully utilize the gradient filter routine (see AIADD Document for more details). The following sections describe the actual input needed to run the ABI-SO<sub>2</sub>.

#### 3.3.1 Primary Sensor Data

The list below contains the primary sensor data currently used by the ABI-SO<sub>2</sub>. By primary sensor data, we mean information that is derived solely from the ABI observations and geolocation information.

- Calibrated radiances for ABI channels 10 (7.4  $\mu\text{m}$ ), 11 (8.5  $\mu\text{m}$ ), 14 (11  $\mu\text{m}$ ), and 15 (12  $\mu\text{m}$ ).
- Calibrated brightness temperatures for ABI channels 8 (6.2  $\mu\text{m}$ ), 10 (7.4  $\mu\text{m}$ ), 11 (8.5  $\mu\text{m}$ ), 14 (11  $\mu\text{m}$ ), and 15 (12  $\mu\text{m}$ )
- Sensor viewing zenith angle
- L1b quality information from calibration for ABI channels 8, 10, 11, 14, and 15
- Space mask (is the pixel geolocated on the surface of the Earth?)

#### 3.3.2 Ancillary Data

The following data lists and briefly describes the ancillary data required to run the ABI-SO<sub>2</sub>. By ancillary data, we mean data that requires information not included in the ABI observations or geolocation data.

- **Cloud frequency of occurrence look-up tables (LUT's)**  
The ABI-SO<sub>2</sub> requires static look-up tables that contain a normalized frequency of occurrence of the joint combination of certain cloud emissivity and cloud microphysical relationships. The look-up table was generated using a Spinning Enhanced Visible Infrared Imager (SEVIRI) based training data set that did not have any SO<sub>2</sub> clouds. The look-up table, which will be provided, is used to help identify pixels that are “spectrally anomalous,” possibly due to the present of SO<sub>2</sub>.

#### 3.3.3 Radiative Transfer Models

The following lists and briefly describes the data that must be calculated by a radiative transfer model and derived prior to running the ABI-SO<sub>2</sub>. See the AIADD Document for a more detailed description.

- **Black cloud radiance profiles for channels 10, 11, 14, and 15**

The ABI-SO<sub>2</sub> requires the radiance emitted upward by a black body surface and transmitted through a non-cloudy atmosphere, with gaseous absorption, to the top of the atmosphere as a function of the atmospheric level of the black surface. The black cloud radiance is computed as a function of NWP grid cells and viewing angle (it is not computed at the pixel resolution), as described in detail in the AIADD Document.

- **Top-of-atmosphere clear-sky radiance estimates for channels 10, 11, 14, and 15**

The ABI-SO<sub>2</sub> requires knowledge of the top-of-atmosphere radiance ABI would sense under clear-sky conditions at each pixel.

- **Top-of-atmosphere clear-sky brightness temperature estimates for channels 8, 10, 11, and 14**

The ABI-SO<sub>2</sub> requires knowledge of the top-of-atmosphere brightness temperature ABI would sense under clear-sky conditions at each pixel.

## 3.4 Theoretical Description

The methodology described in this section is based on some of the physical concepts described in Pavolonis (2010a and 2010b).

### 3.4.1 Physics of the Problem

Figure 2 shows the impact of SO<sub>2</sub> absorption on the infrared spectrum from 6.25 – 9.09 μm. SO<sub>2</sub> absorption is not present or is negligible at higher wavelengths, so wavelengths higher than 9.09 μm are not shown. The spectral bandwidth of ABI channels 10 (7.4 μm) and channel 11 (8.5 μm) are shown on the figure. As can be seen, only channels 10 and 11 are noticeably impacted by SO<sub>2</sub>. As such, “spectral anomalies” due to SO<sub>2</sub> absorption can be detected by inferring when the difference in cloud emissivity (or optical depth) between a channel that is sensitive to SO<sub>2</sub> and a channel that is not sensitive to SO<sub>2</sub> is anomalously large (compared to non-SO<sub>2</sub> clouds).

Previous imager based approaches developed for detecting SO<sub>2</sub> rely largely on empirical relationships. For instance, Prata et al. (2003) and Prata and Kerkmann (2007) spectrally interpolated the observed radiance at 6.2 (or 6.7 μm) and 11 μm to 7.4 μm (to estimate the thermal anomaly potentially induced by SO<sub>2</sub>), and applied some brightness temperature and brightness temperature difference constraints to detect SO<sub>2</sub>. Doutriaux-Boucher and Dubuisson (2008) showed that this empirical method is most effective at unambiguously detecting large amounts of SO<sub>2</sub> (> 50 DU). The GOES-R requirements

state that SO<sub>2</sub> loadings of 10 DU or more are to be detected with an accuracy (skill score) of 70%. As such, the empirical techniques described in the literature are not well suited for addressing the GOES-R SO<sub>2</sub> detection requirements. An alternative approach is to identify large anomalies in cloud microphysics, which are characterized by a large spectral variation in cloud emissivity across SO<sub>2</sub> sensitive and non-SO<sub>2</sub> sensitive channels. In the ABI-SO<sub>2</sub>, the spectral signature of a potential SO<sub>2</sub> cloud is primarily identified using effective absorption optical depth ratios, as described in the following sections. In addition, the ABI-SO<sub>2</sub> utilizes advanced spatial analysis to further improve the SO<sub>2</sub> detection capabilities, as described in later sections.

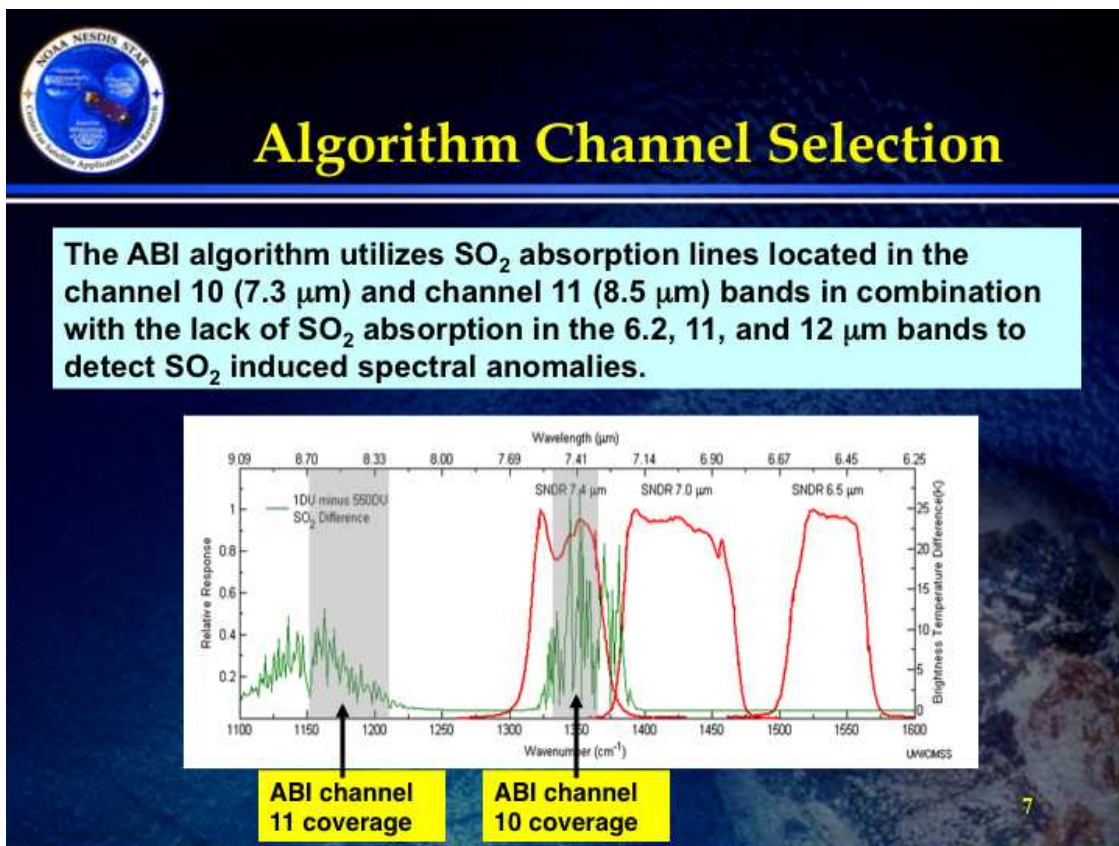


**Figure 2:** Simulated brightness temperature difference between a 1 Dobson Unit (DU) loading of SO<sub>2</sub> and a 550 DU loading as a function of wavelength. The ABI spectral bandwidths for channel 10 (7.4  $\mu\text{m}$ ) and channel 11 (8.5  $\mu\text{m}$ ) are shaded in gray. Wavelengths longer than about 9  $\mu\text{m}$  are not shown since the impact of SO<sub>2</sub> is minimal at those wavelengths. In the infrared, only ABI channels 10 and 11 are significantly impacted by SO<sub>2</sub> absorption.

### 3.4.1.1 Infrared Radiative Transfer

Assuming a satellite viewing perspective (e.g. upwelling radiation), a fully cloudy field of view, a non-scattering atmosphere (no molecular scattering), and a negligible contribution from downwelling cloud emission or molecular emission that is reflected by the surface and transmitted to the top of troposphere (Zhang and Menzel (2002) showed that this term is very small at infrared wavelengths), the cloudy radiative transfer equation for a given infrared channel or wavelength can be written as in Equation 1 (e.g. Heidinger and Pavolonis, 2009; Pavolonis, 2010a).

$$R_{obs}(\lambda) = \epsilon(\lambda)R_{ac}(\lambda) + t_{ac}(\lambda)\epsilon(\lambda)B(\lambda, T_{eff}) + R_{clr}(\lambda)(1 - \epsilon(\lambda)) \quad (\text{Eq. 1})$$

In Equation 1,  $\lambda$  is wavelength,  $R_{obs}$  is the observed top-of-atmosphere (TOA) radiance,  $R_{clr}$  is the TOA clear sky radiance.  $R_{ac}$  and  $t_{ac}$  are the above cloud to TOA upwelling atmospheric radiance and transmittance, respectively.  $B$  is the Planck Function, and  $T_{eff}$  is the effective cloud temperature. The effective cloud emissivity (Cox, 1976) is given by  $\epsilon$ . To avoid using additional symbols, the angular dependence is simply implied. Equation 1, while commonly used, is derived step by step in Pavolonis (2010a), if interested.

Equation 1 can readily be solved for the effective cloud emissivity as follows:

$$\epsilon(\lambda) = \frac{R_{obs}(\lambda) - R_{clr}(\lambda)}{[B(\lambda, T_{eff})t_{ac}(\lambda) + R_{ac}(\lambda)] - R_{clr}(\lambda)} \quad (\text{Eq. 2})$$

In Equation 2, the term in brackets in the denominator is the blackbody cloud radiance that is transmitted to the TOA plus the above cloud (ac) atmospheric radiance. This term is dependent upon the effective cloud vertical location. The cloud vertical location dependence will be discussed in detail in later sections. Other than  $R_{obs}(\lambda)$ , the information needed to evaluate this expression is provided by the output from the clear sky radiative transfer model described in the AIADD Document.

The cloud microphysical signature cannot be captured with the effective cloud emissivity alone for a single spectral channel or wavelength. It is the spectral variation of the effective cloud emissivity that holds the cloud microphysical information. To harness this information, the effective cloud emissivity is used to calculate effective absorption optical depth ratios; otherwise known as  $\beta$ -ratios (see Inoue 1987; Parol et al., 1991; Giraud et al., 1997; and Heidinger and Pavolonis, 2009). For a given pair of spectral emissivities ( $\epsilon(\lambda_1)$  and  $\epsilon(\lambda_2)$ ):

$$\beta_{obs} = \frac{\ln[1 - \epsilon(\lambda_1)]}{\ln[1 - \epsilon(\lambda_2)]} = \frac{\tau_{abs}(\lambda_1)}{\tau_{abs}(\lambda_2)} \quad (\text{Eq. 3})$$

Notice that Equation 3 can simply be interpreted as the ratio of effective absorption optical depth ( $\tau$ ) at two different wavelengths. The word “effective” is used since the

cloud emissivity depends upon the effective cloud temperature. The effective cloud temperature is most often different from the thermodynamic cloud top temperature since the cloud emission originates from a layer in the cloud. The depth of this layer depends upon the cloud transmission profile, which is generally unknown. One must also consider that the effects of cloud scattering are implicit in the cloud emissivity calculation since the actual observed radiance will be influenced by cloud scattering to some degree. In other words, no attempt is made to separate the effects and absorption and scattering. At wavelengths in the 10 to 13  $\mu\text{m}$  range, the effects of cloud scattering for upwelling radiation are quite small and usually negligible. But at infrared wavelengths in the 8 – 10  $\mu\text{m}$  range, the cloud reflectance can make a 1 – 3% contribution to the top of atmosphere radiance (Turner, 2005). Thus, it is best to think of satellite-derived effective cloud emissivity as a radiometric parameter, which, in most cases, is proportional to the fraction of radiation incident on the cloud base that is absorbed by the cloud. See Cox (1976) for an in depth explanation of effective cloud emissivity.

An appealing quality of  $\beta_{\text{obs}}$ , is that it can be interpreted in terms of the single scatter properties, which can be computed for a given cloud composition and particle distribution. Following Van de Hulst (1980) and Parol et al. (1991), a spectral ratio of scaled extinction coefficients can be calculated from the single scatter properties (single scatter albedo, asymmetry parameter, and extinction cross section), as follows.

$$\beta_{\text{theo}} = \frac{[1.0 - \omega(\lambda_1)g(\lambda_1)]\sigma_{\text{ext}}(\lambda_1)}{[1.0 - \omega(\lambda_2)g(\lambda_2)]\sigma_{\text{ext}}(\lambda_2)} \quad (\text{Eq. 4})$$

In Equation 4,  $\beta_{\text{theo}}$  is the spectral ratio of scaled extinction coefficients,  $\omega$  is the single scatter albedo,  $g$  is the asymmetry parameter, and  $\sigma_{\text{ext}}$  is the extinction cross section for an assumed particle distribution. At wavelengths in the 8 – 15  $\mu\text{m}$  range, where multiple scattering effects are small,  $\beta_{\text{theo}}$ , captures the essence of the cloudy radiative transfer such that,

$$\beta_{\text{obs}} \approx \beta_{\text{theo}} \quad (\text{Eq. 5})$$

Equation 4, which was first shown to be accurate for observation in the 10 – 12  $\mu\text{m}$  “window” by Parol et al. (1991), only depends upon the single scatter properties. It does not depend upon the observed radiances, cloud height, or cloud optical depth. By using  $\beta$ -ratios as opposed to brightness temperature differences, we are not only accounting for the non-cloud contribution to the radiances, we are also providing a means to tie the observations back to theoretical size distributions. This framework clearly has practical and theoretical advantages over traditional brightness temperature differences. Parol et al. (1991) first showed that Equation 5 is a good approximation. Pavolonis (2010a) also showed that Equation 5 is a good approximation throughout the 10 - 13  $\mu\text{m}$  window. Faster computers and improvements in the efficiency and accuracy of clear sky radiative transfer modeling have allowed for more detailed exploration of the  $\beta$  data space and computation of  $\beta$ -ratios on a global scale. As such, Pavolonis (2010a) and Pavolonis

(2010b) showed that  $\beta$ -ratios offer improved sensitivity to cloud microphysical properties relative to brightness temperature differences for the same channel pair.

### 3.4.1.2 Converting the Measured Radiances to Emissivities and $\beta$ -Ratios

Given the measured radiances at 7.4, 8.5, 11, and 12  $\mu\text{m}$  (ABI channels 10, 11, 14, and 15) and estimates of the clear sky radiance, clear sky transmittance, and the temperature profile, Equations 2 and 3 are used to compute  $\beta$  for the following spectral pairs: (8.5, 11  $\mu\text{m}$ ), (11, 12  $\mu\text{m}$ ), and (7.4, 11  $\mu\text{m}$ ). Given these spectral pairs, the 11  $\mu\text{m}$  emissivity is always placed in the denominator of Equation 3. Hereafter, these  $\beta$ 's are referred to as  $\beta(8.5/11\mu\text{m})$ ,  $\beta(12/11\mu\text{m})$ , and  $\beta(7.4/11\mu\text{m})$ , respectively. The only missing piece of information is the effective cloud vertical level, which is needed in computing the cloud emissivity. The effective cloud vertical level is the level where the temperature profile is equal to the extinction weighted cloud temperature. As shown in Pavolonis (2010a) and Pavolonis (2010b), the sensitivity of  $\beta$  to the effective cloud vertical level is often small when “window” channel pairs are used. As such, cloud microphysical information can be gleaned even by assuming a constant effective cloud vertical level. The retrieval of the actual effective cloud vertical level is unnecessary for this application and beyond the scope of this algorithm. In addition, the cloud composition must also be known to properly constrain the cloud microphysics in a formal retrieval of the cloud vertical level. That is why the ABI-SO<sub>2</sub> algorithm must work in the absence of cloud height information.

The ABI-SO<sub>2</sub> algorithm assumes a constant effective cloud level consistent with the thermodynamic tropopause given by Numerical Weather Prediction (NWP) data (see the AIADD Document for more information). Equations 6a – 6g specifically show how this assumption is applied to Equations 2 and 3 for the channel pairs used in the ABI-SO<sub>2</sub>. In these equations,  $\epsilon_{\text{stropo}}(\lambda)$  is the spectral cloud emissivity computed using the single layer tropopause assumption, and  $\beta_{\text{stropo}}(\lambda_1/\lambda_2)$  represents the  $\beta$  calculated from this type of cloud emissivity.  $T_{\text{tropo}}$  is the temperature of the tropopause.  $R_{\text{tropo}}(\lambda)$  and  $t_{\text{tropo}}(\lambda)$  are the clear sky atmospheric radiance and transmittance, vertically integrated from the tropopause to the top of the atmosphere, respectively (the calculation of the clear sky radiance and transmittance are described in detail in the AIADD Document). All other terms were defined previously. Pavolonis (2010a) showed that the top of troposphere cloud height assumption is mainly useful for “window” channels. However, SO<sub>2</sub> clouds, that can be sensed with the 7.4  $\mu\text{m}$  channel, are often located near the tropopause, so the top of troposphere assumption is quite reasonable for the  $\beta(7.4/11\mu\text{m})$ , even though the 7.4  $\mu\text{m}$  channel is subject to significant water vapor absorption.

$$\epsilon_{\text{stropo}}(7.4\mu\text{m}) = \frac{R_{\text{obs}}(7.4\mu\text{m}) - R_{\text{clr}}(7.4\mu\text{m})}{[B(7.4\mu\text{m}, T_{\text{tropo}})t_{\text{tropo}}(7.4\mu\text{m}) + R_{\text{tropo}}(7.4\mu\text{m})] - R_{\text{clr}}(7.4\mu\text{m})} \quad (\text{Eq. 6a})$$

$$\epsilon_{stropo}(8.5\mu m) = \frac{R_{obs}(8.5\mu m) - R_{clr}(8.5\mu m)}{[B(8.5\mu m, T_{tropo})t_{tropo}(8.5\mu m) + R_{tropo}(8.5\mu m)] - R_{clr}(8.5\mu m)} \quad (\text{Eq. 6b})$$

$$\epsilon_{stropo}(11\mu m) = \frac{R_{obs}(11\mu m) - R_{clr}(11\mu m)}{[B(11\mu m, T_{tropo})t_{tropo}(11\mu m) + R_{tropo}(11\mu m)] - R_{clr}(11\mu m)} \quad (\text{Eq. 6c})$$

$$\epsilon_{stropo}(12\mu m) = \frac{R_{obs}(12\mu m) - R_{clr}(12\mu m)}{[B(12\mu m, T_{tropo})t_{tropo}(12\mu m) + R_{tropo}(12\mu m)] - R_{clr}(12\mu m)} \quad (\text{Eq. 6d})$$

$$\beta_{stropo}(8.5/11\mu m) = \frac{\ln[1 - \epsilon_{stropo}(8.5\mu m)]}{\ln[1 - \epsilon_{stropo}(11\mu m)]} \quad (\text{Eq. 6e})$$

$$\beta_{stropo}(12/11\mu m) = \frac{\ln[1 - \epsilon_{stropo}(12\mu m)]}{\ln[1 - \epsilon_{stropo}(11\mu m)]} \quad (\text{Eq. 6f})$$

$$\beta_{stropo}(7.4/11\mu m) = \frac{\ln[1 - \epsilon_{stropo}(7.4\mu m)]}{\ln[1 - \epsilon_{stropo}(11\mu m)]} \quad (\text{Eq. 6g})$$

### 3.4.1.3 Clouds in $\beta$ -Space

As discussed in Section 3.4.1, pure SO<sub>2</sub> gas clouds do not appreciably absorb infrared radiation outside of the 7.4 and 8.5  $\mu m$  bands. Thus, pure SO<sub>2</sub> clouds cannot be sensed with the 11 and 12  $\mu m$  channels. However, clouds that contain SO<sub>2</sub> generally also contain water (liquid and/or ice) and/or volcanic ash (water and ash absorb radiation throughout the infrared spectrum) or overlap lower level water (liquid and/or ice) or volcanic ash clouds. Thus, the measured 11 and 12  $\mu m$  channel radiance is generally smaller than the corresponding clear sky radiance, and the 11 and 12  $\mu m$  cloud emissivity will be  $> 0.0$  (resulting in numerically valid  $\beta_{stropo}(12/11\mu m)$ ,  $\beta_{stropo}(8.5/11\mu m)$ , and  $\beta_{stropo}(7.4/11\mu m)$  values). “Pure” SO<sub>2</sub> clouds do occasionally occur. As described in Section 3.4.2.1.2, these clouds are spectrally identified using an alternative methodology, but most SO<sub>2</sub> clouds can be identified using the various  $\beta_{stropo}$  parameters.

To illustrate how SO<sub>2</sub> clouds differ from other types of clouds in  $\beta$ -space, example SO<sub>2</sub>, liquid water, ice, and dust clouds were manually selected from a SEVIRI full disk image, and the values of  $\beta_{stropo}(12/11\mu m)$ ,  $\beta_{stropo}(8.5/11\mu m)$ , and  $\beta_{stropo}(7.4/11\mu m)$  were examined. The selected clouds, which were identified using false color multi-spectral imagery, are shown in Figure 3. The 2-dimensional distributions of  $\beta_{stropo}(12/11\mu m)$  vs.  $\beta_{stropo}(8.5/11\mu m)$  and  $\beta_{stropo}(8.5/11\mu m)$  vs.  $\beta_{stropo}(7.4/11\mu m)$  for each selected cloud are shown in Figure 4 and Figure 5, respectively. As Figure 4 and Figure 5 show, SO<sub>2</sub> clouds generally have different joint  $\beta_{stropo}$  signatures than other types of clouds. The  $\beta_{stropo}(7.4/11\mu m)$  is generally much larger for SO<sub>2</sub> clouds compared to other clouds due to the strong SO<sub>2</sub> absorption lines contained in this band. The SO<sub>2</sub> absorption significantly increases the 7.4  $\mu m$  absorption cloud optical depth relative to the 11  $\mu m$  absorption

cloud optical depth, resulting in a  $\beta_{\text{stropo}}(7.4/11\mu\text{m})$  that is much larger compared to other cloud types. The same reasoning applies to the  $\beta_{\text{stropo}}(8.5/11\mu\text{m})$ . Accordingly,  $\beta_{\text{stropo}}(8.5/11\mu\text{m})$  also tends to be larger for SO<sub>2</sub> compared to other cloud types, but is a bit more complicated to interpret when the SO<sub>2</sub> cloud overlaps lower non-SO<sub>2</sub> cloud layers, which, based on visual inspection of multi-spectral imagery, is a common occurrence. The 8.5  $\mu\text{m}$  channel has a weighting function that peaks in the lower troposphere, as such it is far more sensitive to the presence of low non-SO<sub>2</sub> cloud layers than the 7.4  $\mu\text{m}$  channel. Lower non-SO<sub>2</sub> cloud layers that lie beneath an SO<sub>2</sub> cloud layer will generally act to decrease the difference in cloud optical depth between the 8.5 and 11  $\mu\text{m}$  channels compared to a single layer SO<sub>2</sub> cloud, resulting in decreased  $\beta_{\text{stropo}}(8.5/11\mu\text{m})$  contrast (between SO<sub>2</sub> features and non-SO<sub>2</sub> features). Further, the liquid water and dust clouds chosen in this scene reside well beneath the peak of the 7.4  $\mu\text{m}$  atmospheric weighting function and thus cannot be detected with this channel (which is relevant information since SO<sub>2</sub> clouds generally can be detected with the 7.4  $\mu\text{m}$  channel). The  $\beta_{\text{stropo}}(12/11\mu\text{m})$  is not directly sensitive to SO<sub>2</sub>, but is very sensitive to the size of cloud water particles (e.g. Pavolonis 2010a). SO<sub>2</sub> clouds that contain liquid water or ice tend to be composed of small particles, which results in a larger  $\beta_{\text{stropo}}(12/11\mu\text{m})$  compared to most meteorological clouds. Figure 4 shows that many pixels in the SO<sub>2</sub> cloud have larger values of  $\beta_{\text{stropo}}(12/11\mu\text{m})$  relative to the liquid water and ice clouds that were analyzed.

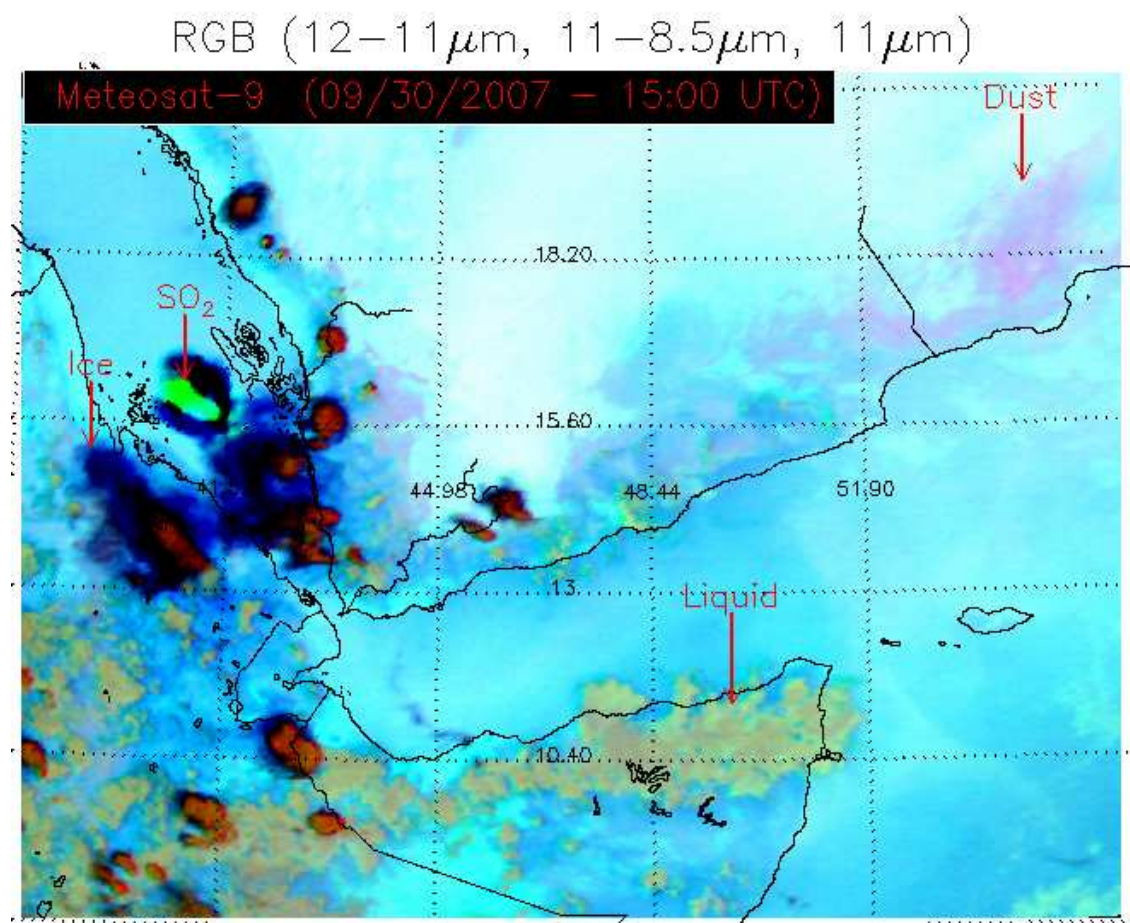


**Figure 3:** A false color SEVIRI image (September 30, 2007, 1500 UTC) indicating the location of the ice, liquid water, dust, and SO<sub>2</sub> clouds selected to illustrate the multi-spectral microphysical signal exhibited by different cloud type.

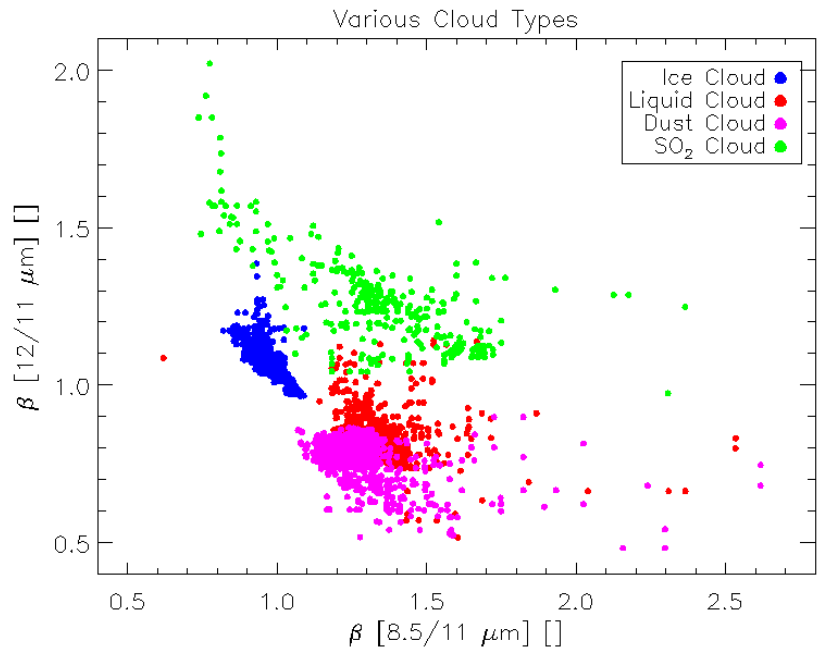


**Figure 4: The 2D distribution of  $\beta_{\text{stropo}}(8.5/11 \mu\text{m})$  and  $\beta_{\text{stropo}}(12/11 \mu\text{m})$  for 4 different cloud types (ice, liquid water, dust, and  $\text{SO}_2$ ) observed by SEVIRI on September 30, 2007 at 1500 UTC.**

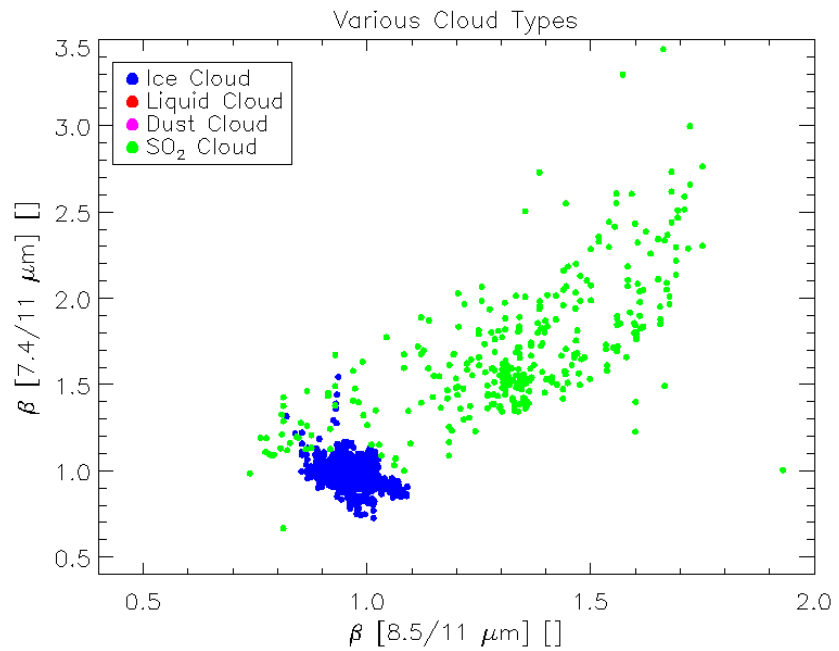


**Figure 5: The 2D distribution of  $\beta_{\text{stropo}}(8.5/11 \mu\text{m})$  and  $\beta_{\text{stropo}}(7.4/11 \mu\text{m})$  for 4 different cloud types (ice, liquid water, dust, and  $\text{SO}_2$ ) observed by SEVIRI on September 30, 2007 at 1500 UTC. The absence of liquid water and dust data points**

**indicates that those clouds were too low in the atmosphere to be sensed by the 7.4  $\mu\text{m}$  channel.**

#### 3.4.1.4 Identifying a Pixel's Local Radiative Center

In regions where the radiative signal of a cloud is small, like cloud edges, the various  $\beta$ -ratios are difficult to interpret since the cloud fraction, which is assumed to be 1.0, may be less than 1.0, or very small cloud optical depths may produce a signal that cannot be differentiated from noise. With the spectral information limited, a spatial metric is needed to make a spatially and physically consistent  $\text{SO}_2$  determination for these types of pixels. To address this problem, the gradient filter procedure, which is described in detail in the AIADD Document, is used to determine the Local Radiative Center (LRC) of each valid pixel. A pixel is valid if it has a valid Earth latitude and longitude and has valid spectral data (based on the L1b calibration flags). The  $\epsilon_{\text{stropo}}(11\mu\text{m})$  parameter described in Section 3.4.1.2 is used to compute the LRC. The gradient filter inputs (which are described in detail in the AIADD Document) for this application are listed in Table 3.

| Gradient Variable                         | Minimum Valid Value of Gradient Variable | Maximum Valid Value of Gradient Variable | Gradient Stop Value | Apply Gradient Filter To  |
|---|--|--|---------------------|---|
| $\epsilon_{\text{stropo}}(11\mu\text{m})$ | 0.0                                      | 1.0                                      | 0.7                 | All pixels with a valid Earth lat/lon and valid spectral data for ABI channels 10, 11, 14, and 15 |

**Table 3: Inputs used in calculation of Local Radiative Center (LRC). The gradient filter function used in the calculation is described in the AIADD document.**

The gradient filter allows one to consult the spectral information at an interior pixel within the same cloud in order to avoid using the spectral information offered by pixels with a very weak cloud radiative signal or sub-pixel cloudiness associated with cloud edges. Overall, this use of spatial information allows for a more spatially and physically consistent product. This concept is also explained in Pavolonis (2010b).

#### 3.4.1.5 Cloud Objects

The  $\text{SO}_2$  detection is performed on a cloud object basis. A cloud object is defined as a collection of spatially connected pixels that meet application dependent criteria (e.g. in the case of  $\text{SO}_2$ , pixels that are characterized by large microphysical anomalies). Wielicki and Welch (1986) first used satellite derived cloud objects to study small-scale cumulus cloud properties. In the  $\text{SO}_2$  detection algorithm, cloud objects are constructed from candidate  $\text{SO}_2$  pixels, which are objectively identified using spectral information. A series of filters (simple logical tests) are applied to each cloud object, where various

cloud object statistics are used to filter out non-SO<sub>2</sub> cloud objects. Most true SO<sub>2</sub> cloud objects will be composed of SO<sub>2</sub> pixels that exhibit a non-ambiguous SO<sub>2</sub> spectral signature as well as pixels that contain SO<sub>2</sub> but exhibit a marginal SO<sub>2</sub> spectral signature, which cannot be cleanly distinguished from all other non-SO<sub>2</sub> features. The cloud object procedure is very powerful because it provides a mechanism to accurately identify pixels that contain SO<sub>2</sub>, but do not have a totally unique spectral signature, on the basis that those pixels are spatially connected to pixels that do exhibit a robust spectral signature. The specific methodology for constructing cloud objects and the cloud object filtering will be described in detail in upcoming sections of this document.

#### **3.4.1.6 Median Spatial Filter**

The emissivity and  $\beta$  calculations described in Section 3.4.1.2 can, at times, be noisy, especially near cloud edges, in areas of broken clouds, and for very small cloud optical depths. In order to minimize the occurrence of “salt and pepper” noise, a standard 3 x 3 median filter is applied to certain key variables ( $\epsilon_{\text{stropo}}(7.4\mu\text{m})$ ,  $\epsilon_{\text{stropo}}(11\mu\text{m})$ , and the cloud object membership flag variables). The median filter simply replaces the value at each pixel with the median value of a 3 x 3 pixel array centered on that pixel. The generic median filter procedure is described in the AIADD Document.

### **3.4.2 Mathematical Description**

While Section 3.4.1 focused on describing the physical basis of the SO<sub>2</sub> detection algorithm, this section is dedicated to describing the logic needed to implement the ABI-SO<sub>2</sub>.

#### **3.4.2.1 Cloud Object Membership Criteria**

Before the cloud objects can be constructed, a cloud object mask must be created to identify pixels that meet the object membership criteria. In the ABI-SO<sub>2</sub>, two sets of cloud objects are created. One set of cloud objects is formed from pixels that exhibit a rare cloud microphysical signal determined from a frequency of occurrence look-up table. The first set of objects will be referred to as “beta objects.” The second set of cloud objects is composed from pixels that have a weak cloud signal, inferred from cloud emissivity variables and brightness temperature differences, in non-SO<sub>2</sub> absorption channels (e.g. 11  $\mu\text{m}$ ). The second set of objects will be referred to as “btd objects.” The methodology of Wielicki and Welch (1986) is used to construct cloud objects and the object membership criteria are described in the sections below.

##### ***3.4.2.1.1 “Beta Object” Membership Criteria***

Using a SEVIRI based offline training data set that did not contain any detectable SO<sub>2</sub> clouds, the joint frequency of occurrence is determined for two different  $\beta_{\text{stropo}}$  pairs, ( $\beta_{\text{stropo}}(8.5/11\mu\text{m})$ ,  $\beta_{\text{stropo}}(12/11\mu\text{m})$ ) and ( $\beta_{\text{stropo}}(8.5/11\mu\text{m})$ ,  $\beta_{\text{stropo}}(7.4/11\mu\text{m})$ ). The frequency of occurrence look-up tables, which are based on 8 full disks of SEVIRI (1 x 10<sup>8</sup> pixels), are three dimensional. The 8 SEVIRI full disks include data from each season at 00 and 12 UTC. The first look-up table (LUT1) has the following physical dimensions:  $\epsilon_{\text{stropo}}(8.5 \mu\text{m}) \times \beta_{\text{stropo}}(8.5/11\mu\text{m}) \times \beta_{\text{stropo}}(12/11\mu\text{m})$ . The second look-up table (LUT2) has the following physical dimensions:  $\epsilon_{\text{stropo}}(7.4 \mu\text{m}) \times \beta_{\text{stropo}}(8.5/11\mu\text{m}) \times \beta_{\text{stropo}}(7.4/11\mu\text{m})$ . The look-up tables are visualized in Figure 6 and Figure 7. In both look-up tables, the frequency of occurrence is defined as the count in each 2D histogram bin divided by the maximum bin count in the entire table. Since we are only interested in spectral anomalies associated with SO<sub>2</sub> absorption, the borders of the look-up tables are constrained. For LUT1, a valid cloud frequency of occurrence is retrieved from the look-up table if  $\epsilon_{\text{stropo}}(8.5 \mu\text{m}) > 0.05$ ,  $\beta_{\text{stropo}}(8.5/11\mu\text{m})$  and  $\beta_{\text{stropo}}(12/11\mu\text{m})$  have valid (non-missing) values, and the 11 – 12  $\mu\text{m}$  brightness temperature difference is greater than 0.50 K. For LUT2, a valid cloud frequency of occurrence is retrieved from the look-up table if  $\epsilon_{\text{stropo}}(8.5 \mu\text{m}) > 0.01$ ,  $\epsilon_{\text{stropo}}(7.4 \mu\text{m}) > 0.01$ ,  $\beta_{\text{stropo}}(8.5/11\mu\text{m})$  and  $\beta_{\text{stropo}}(7.4/11\mu\text{m})$  have valid (non-missing) values, and the 8.5 – 11  $\mu\text{m}$  brightness temperature difference is less than 0.00 K. The brightness temperature difference constraints assure that any low frequency of occurrence is more likely to be associated with SO<sub>2</sub> rather than some other feature. The final frequency of occurrence assigned to each pixel is the minimum valid frequency of occurrence retrieved from LUT1 and LUT2. If the final pixel frequency of occurrence is valid and less than 0.01, then the “beta object” membership requirements are fulfilled and that pixel is used to construct “beta objects;” otherwise the pixel cannot be used to construct “beta objects.”

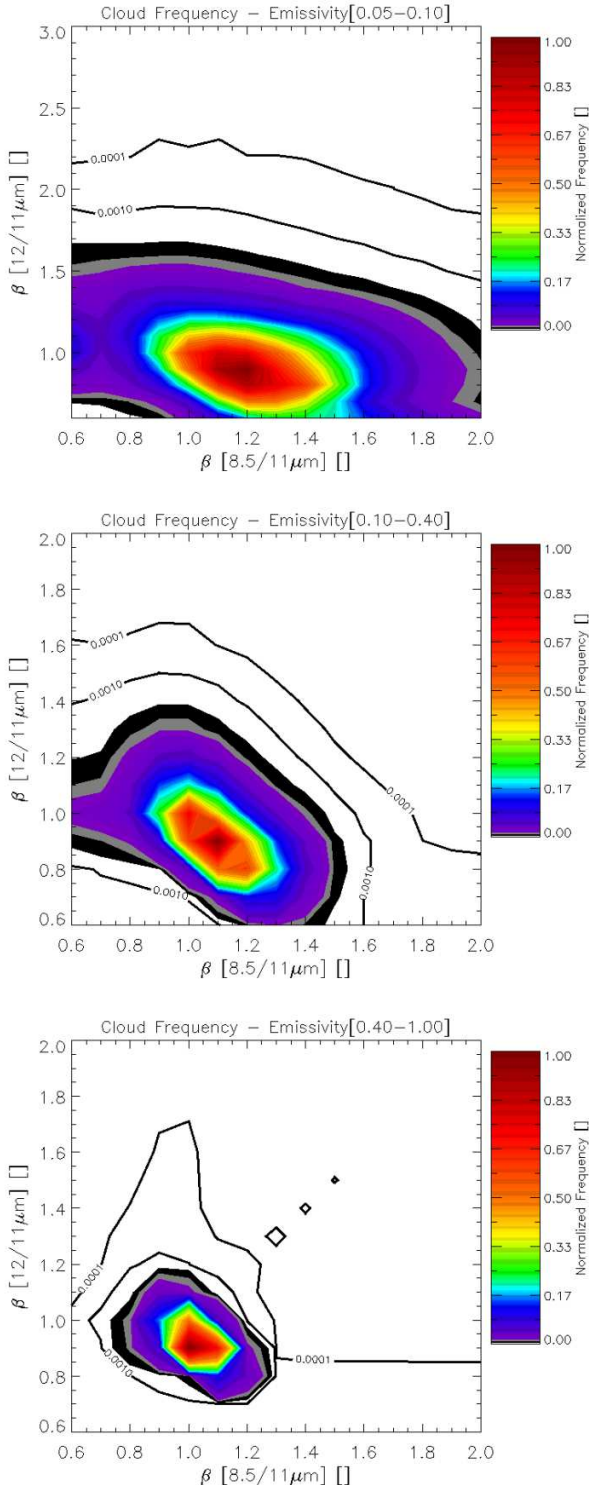


**Figure 6:** The normalized joint frequency of occurrence of  $\beta_{\text{stropo}}(8.5/11\mu\text{m})$  and  $\beta_{\text{stropo}}(12/11\mu\text{m})$  for three different  $\epsilon_{\text{stropo}}(8.5 \mu\text{m})$  bins.

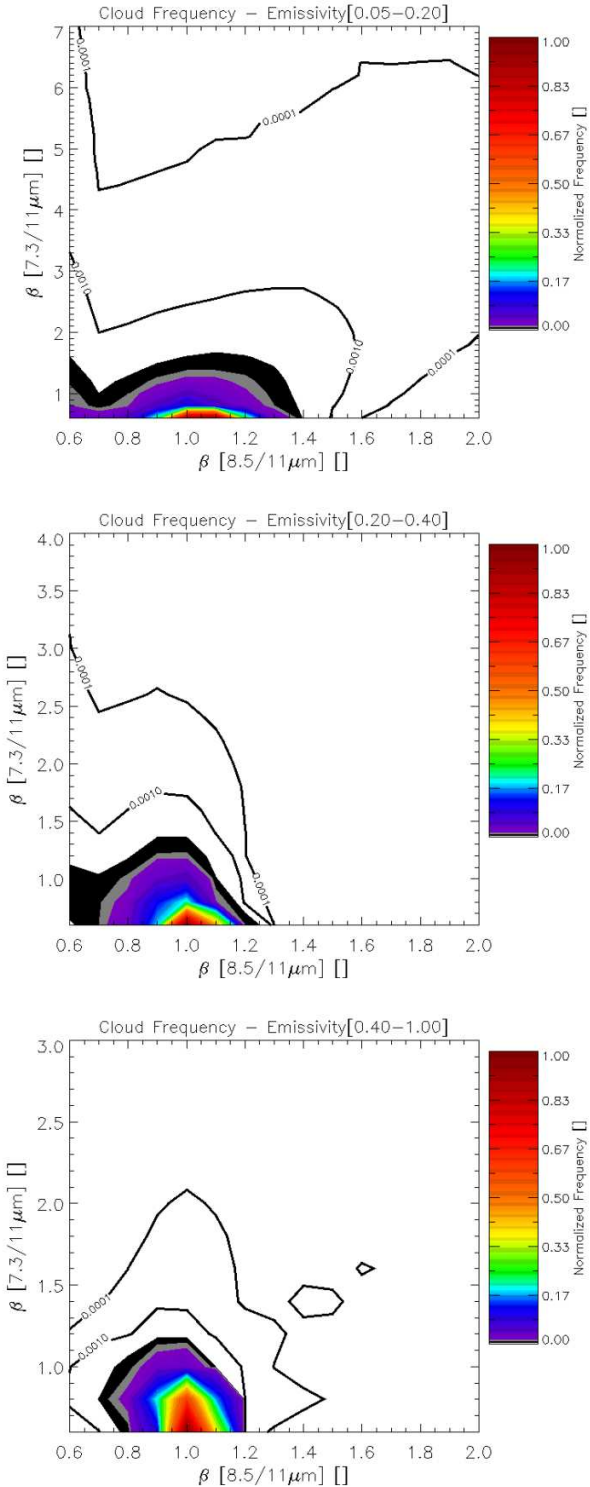


**Figure 7: The normalized joint frequency of occurrence of  $\beta_{\text{stropo}}(8.5/11\mu\text{m})$  and  $\beta_{\text{stropo}}(7.3/11\mu\text{m})$  for three different  $\epsilon_{\text{stropo}}(7.4 \mu\text{m})$  bins.**

### **3.4.2.1.2 “Btd Object” Membership Criteria**

A second separate set of objects is constructed using alternative criteria for object membership, with the goal of detecting “pure” SO<sub>2</sub> clouds. The object membership criteria are satisfied *if at least one of two sets of conditions is true*. The two sets of conditions are defined below in pseudo-code form.

#### **First set of conditions:**

**IF** ( $\epsilon_{\text{stropo}}(7.4 \mu\text{m}) > 0.04$  **AND**  $\epsilon_{\text{stropo}}(11 \mu\text{m}) < 0.05$ ) **THEN**  
-object membership criteria met

#### **Second set of conditions:**

New variable definitions:

**BTD(8.5-11 μm)** = the observed 8.5 μm – 11 μm brightness temperature difference

**BTD\_CLR(8.5-11 μm)** = the calculated clear sky 8.5 μm – 11 μm brightness temperature difference

**BTD(7.4-6.2 μm)** = the observed 7.4 μm – 6.2 μm brightness temperature difference

**BTD\_CLR(7.4-6.2 μm)** = the calculated clear sky 7.4 μm – 6.2 μm brightness temperature difference

**IF** (( $\epsilon_{\text{stropo}}(7.4 \mu\text{m}) > 0.01$  **OR**  $\epsilon_{\text{stropo}}(8.5 \mu\text{m}) > 0.01$ ) **AND**  
( $\epsilon_{\text{stropo}}(7.4 \mu\text{m}) > \epsilon_{\text{stropo}}(11 \mu\text{m})$  **OR**  $\epsilon_{\text{stropo}}(8.5 \mu\text{m}) > \epsilon_{\text{stropo}}(11 \mu\text{m})$ ) **AND**  
( $\text{BTD}(8.5-11 \mu\text{m}) < -3.0 \text{ K}$ ) **AND**  
( $\text{BTD}(7.4 - 6.2 \mu\text{m}) < \text{BTD\_CLR}(7.4 - 6.2 \mu\text{m}) - 1.0 \text{ K}$ ) **AND**  
( $\text{BTD}(8.5 - 11 \mu\text{m}) < \text{BTD\_CLR}(8.5 - 11 \mu\text{m}) - 1.0 \text{ K}$ ) **THEN**  
-object membership criteria met

### **3.4.2.1.3 Cloud Object Statistics**

As object eligible pixels are sorted into cloud objects, object statistics are tabulated for use in the object filtering. For each set of cloud objects (“beta objects” and “btd objects”), a set of statistics is generated. These statistics are described below.

#### **3.4.2.1.3.1 “Beta Object” Statistics**

The statistics listed in Table 4 need to be generated in order to filter out false alarm “beta objects.”

| <b>Object Statistic</b>  | <b>Purpose</b>  |
|--|---|
| Maximum value of $\epsilon_{\text{stropo}}(7.4 \mu\text{m})$<br><b>[<math>\epsilon_{\text{stropo}}(7.4 \mu\text{m})\_max</math>]</b>                                 | If $\text{SO}_2$ is present this variable is an indication of the strength of the $\text{SO}_2$ absorption at $7.4 \mu\text{m}$   |
| $90^{\text{th}}$ percentile value of $\epsilon_{\text{stropo}}(7.4 \mu\text{m})$<br><b>[<math>\epsilon_{\text{stropo}}(7.4 \mu\text{m})\_p90</math>]</b>             | This variable is used in conjunction with the $10^{\text{th}}$ percentile value of $\epsilon_{\text{stropo}}(7.4 \mu\text{m})$ to infer information about the width of the $\epsilon_{\text{stropo}}(7.4 \mu\text{m})$ distribution |
| $10^{\text{th}}$ percentile value of $\epsilon_{\text{stropo}}(7.4 \mu\text{m})$<br><b>[<math>\epsilon_{\text{stropo}}(7.4 \mu\text{m})\_p10</math>]</b>             | This variable is used in conjunction with the $90^{\text{th}}$ percentile value of $\epsilon_{\text{stropo}}(7.4 \mu\text{m})$ to infer information about the width of the $\epsilon_{\text{stropo}}(7.4 \mu\text{m})$ distribution |
| $95^{\text{th}}$ percentile value of $\beta_{\text{stropo}}(8.5/11\mu\text{m})$<br><b>[<math>\beta_{\text{stropo}}(8.5/11\mu\text{m})\_p95</math>]</b>               | The purpose of this metric is to determine if at least some pixels have very large values of $\beta_{\text{stropo}}(8.5/11\mu\text{m})$   |
| $95^{\text{th}}$ percentile value of $\beta_{\text{stropo}}(7.4/11\mu\text{m})$<br><b>[<math>\beta_{\text{stropo}}(7.4/11\mu\text{m})\_p95</math>]</b>               | The purpose of this metric is to determine if at least some pixels have very large values of $\beta_{\text{stropo}}(7.4/11\mu\text{m})$   |
| Number of pixels in the object that have a Local Radiative Center (LRC) pixel that meets the “beta object” criteria<br><b>[lrc_count]</b>                            | This statistic is used to help eliminate false alarms that can occur at the edges of meteorological clouds  |
| Number of pixels in the object that have a $\epsilon_{\text{stropo}}(11 \mu\text{m}) > 0.0$<br><b>[<math>\epsilon_{\text{stropo}}(11 \mu\text{m})\_count</math>]</b> | This metric is used to infer how many pixels in the object may contain “pure” $\text{SO}_2$ , which does not absorb at $11 \mu\text{m}$   |

**Table 4:** The object statistics needed to filter out false alarm “beta objects.” The symbols used to denote the individual statistics is shown in bold in the first column.

#### 3.4.2.1.3.2 “Btd Object” Statistics

The statistics listed in **Table 5** need to be generated in order to filter out false alarm “btd objects.”

| Object Statistic   | Purpose   |
|--|---|
| Maximum value of<br>$\epsilon_{\text{stropo}}(7.4 \mu\text{m})$<br><b>[<math>\epsilon_{\text{stropo}}(7.4 \mu\text{m})</math>_max]</b>                   | If $\text{SO}_2$ is present this variable is an indication of the strength of the $\text{SO}_2$ absorption at 7.4 $\mu\text{m}$         |
| 95 <sup>th</sup> percentile value of<br>$\beta_{\text{stropo}}(8.5/11\mu\text{m})$<br><b>[<math>\beta_{\text{stropo}}(8.5/11\mu\text{m})</math>_p95]</b> | The purpose of this metric is to determine if at least some pixels have very large values of $\beta_{\text{stropo}}(8.5/11\mu\text{m})$ |
| 95 <sup>th</sup> percentile value of<br>$\beta_{\text{stropo}}(7.4/11\mu\text{m})$<br><b>[<math>\beta_{\text{stropo}}(7.4/11\mu\text{m})</math>_p95]</b> | The purpose of this metric is to determine if at least some pixels have very large values of $\beta_{\text{stropo}}(7.4/11\mu\text{m})$ |
| Minimum value of the observed 8.5 – 11 $\mu\text{m}$ brightness temperature difference<br><b>[BTD(8.5-11 <math>\mu\text{m}</math>)_Min]</b>              | True $\text{SO}_2$ clouds will have at least some pixels that have strongly negative values of BTD(8.5-11 $\mu\text{m}$ )               |

**Table 5: The object statistics needed to filter out false alarm “btd objects.” The symbols used to denote the individual statistics is shown in bold in the first column.**

#### 3.4.2.1.4 Cloud Object Filters

The “beta objects” and “btd objects” are each separately filtered to eliminate non- $\text{SO}_2$  objects. Each object that survives the filtering is considered an  $\text{SO}_2$  cloud, meaning that the  $\text{SO}_2$  detection mask is set to true ( $\text{SO}_2$  is present) for all pixels that compose the objects that are not filtered out. Whether an  $\text{SO}_2$  cloud is detected using “beta objects” or “btd objects” or both does not matter, as long as it is detected in at least one of the objects sets. A detailed description of the object filters is given in the following sections.

##### 3.4.2.1.4.1 “Beta Object” Filters

The “beta objects” are subjected to five simple logical tests. If all five tests are passed (return “true”), then all of the pixels in the object are deemed to contain  $\text{SO}_2$ . The logical tests are expressed in the table below. All symbols used in the logical tests were defined previously (see Table 4 and Section 3.4.1). The threshold values used in the logical tests were chosen based on the analysis of a set of training objects.

| Test Number | Test Logic   |
|-------------|--|
| 1           | <b>IF</b> (( $\epsilon_{\text{stropo}}(7.4 \mu\text{m})_{\text{max}} > 0.20$ ) <b>OR</b><br>$(\epsilon_{\text{stropo}}(7.4 \mu\text{m})_{\text{max}} > 0.14 \text{ AND } \beta_{\text{stropo}}(8.5/11\mu\text{m})_{\text{p95}} > 2.16 \text{ AND }$<br>$\beta_{\text{stropo}}(7.4/11\mu\text{m})_{\text{p95}} > 2.16)$ ) <b>THEN</b><br><b>Result = true</b> |
| 2           | <b>IF</b> (( $\beta_{\text{stropo}}(8.5/11\mu\text{m})_{\text{p95}} > 2.16$ ) <b>OR</b><br>$(\beta_{\text{stropo}}(8.5/11\mu\text{m})_{\text{p95}} > 1.60 \text{ AND } \epsilon_{\text{stropo}}(7.4 \mu\text{m})_{\text{max}} > 0.30)$ ) <b>THEN</b><br><b>Result = true</b>   |
| 3           | <b>IF</b> (( $\beta_{\text{stropo}}(7.4/11\mu\text{m})_{\text{p95}} > 2.16$ ) <b>OR</b><br>$(\beta_{\text{stropo}}(7.4/11\mu\text{m})_{\text{p95}} > 2.15 \text{ AND } \epsilon_{\text{stropo}}(7.4 \mu\text{m})_{\text{max}} > 0.30)$ ) <b>THEN</b><br><b>Result = true</b>   |
| 4           | Let, $\epsilon_{\text{ratio}} = [\epsilon_{\text{stropo}}(7.4 \mu\text{m})_{\text{p90}} - \epsilon_{\text{stropo}}(7.4 \mu\text{m})_{\text{p10}}] / \epsilon_{\text{stropo}}(7.4 \mu\text{m})_{\text{p90}}$<br><b>IF</b> ( $\epsilon_{\text{ratio}} > 0.25$ ) <b>THEN</b><br><b>Result = true</b>  |
| 5           | Let, $\text{lrc\_ratio} = \text{lrc\_count} / \epsilon_{\text{stropo}}(11 \mu\text{m})_{\text{count}}$<br><b>IF</b> ( $\text{lrc\_ratio} > 0.50$ ) <b>THEN</b><br><b>Result = true</b>   |

**Table 6:** The logical tests used to determine if a “beta object” is an SO<sub>2</sub> cloud are shown. If all five logical tests return “true,” then the object is deemed to be SO<sub>2</sub>; otherwise it is filtered out.

#### 3.4.2.1.4.2 “Btd Object” Filters

The “btd objects” are subjected to four simple logical tests. If all four tests are passed (return “true”), then all of the pixels in the object are deemed to contain SO<sub>2</sub>. The logical tests are expressed in the table below. All symbols used in the logical tests were defined previously (see **Table 5** and Section 3.4.1). The threshold values used in the logical tests were chosen based on the analysis of a set of training objects.

| Test Number | Test Logic  |
|-------------|---|
| 1           | <b>IF</b> ( $\varepsilon_{\text{stropo}}(7.4 \mu\text{m})_{\text{max}} > 0.20$ ) <b>THEN</b><br><b>Result = true</b>  |
| 2           | <b>IF</b> (( $\beta_{\text{stropo}}(8.5/11\mu\text{m})_{\text{p95}} > 2.15$ ) <b>OR</b><br>( $\beta_{\text{stropo}}(8.5/11\mu\text{m})_{\text{p95}} > 2.12$ <b>AND</b> $\varepsilon_{\text{stropo}}(7.4 \mu\text{m})_{\text{max}} > 0.40$ ) <b>THEN</b><br><b>Result = true</b> |
| 3           | <b>IF</b> ( $\beta_{\text{stropo}}(7.4/11\mu\text{m})_{\text{p95}} > 2.16$ ) <b>THEN</b><br><b>Result = true</b>  |
| 4           | <b>IF</b> ( $\text{BTD}(8.5-11 \mu\text{m})_{\text{min}} < -5.0$ ) <b>THEN</b><br><b>Result = true</b>  |

**Table 7:** The logical tests used to determine if a “btd object” is an SO<sub>2</sub> cloud are shown. If all four logical tests return “true,” then the object is deemed to be SO<sub>2</sub>; otherwise it is filtered out.

### 3.4.3 Algorithm Output

#### 3.4.3.1 Product Output

The ABI-SO<sub>2</sub> derives the following ABI products listed in the F&PS.

- SO<sub>2</sub> Detection Mask [SO<sub>2</sub> present = 1 or SO<sub>2</sub> not present = 0]

#### 3.4.3.2 Quality Flag (QF) Output

The ABI-SO<sub>2</sub> produces quality flags. Table 8 describes the SO<sub>2</sub> detection QF flags.

| Byte | Bit | Name                    | Values   |
|------|-----|-------------------------|--|
| 1    | 1   | Overall QF              | 0 – High Quality<br>1 – Low Quality                              |
| 1    | 2   | Invalid Data QF         | 0 – High Quality<br>1 – Low Quality                              |
| 1    | 3   | SatZenith QF            | 0 – High Quality<br>1 – Low Quality                              |
| 1    | 4-5 | SO <sub>2</sub> Loading | 0 – Low Loading<br>1 – Intermediate Loading<br>2 – Heavy Loading |

**Table 8:** SO<sub>2</sub> Detection Quality Flag (QF) description. The Ash Detection QF Flags are bit packed byte variables. The byte column identifies the byte number(s) the QF is stored in and the Bit column lists the bit(s) the flag encompasses within the byte(s). The name of the each flag is included, along with possible values; the bold values are the initialized values.

### 3.4.3.3 Product Quality Information (PQI)

The ABI-SO<sub>2</sub> produces Product Quality Information (PQI). Table 9 describes the PQI.

| Byte | Bit | Name                           | Values                |
|------|-----|--------------------------------|-----------------------|
| 1    | 1   | Pixel is part of “Beta Object” | 0 – False<br>1 – True |
| 1    | 2   | Pixel is part of “BTD Object”  | 0 – False<br>1 - True |

**Table 9: SO<sub>2</sub> detection PQI Flag description.** The SO<sub>2</sub> detection PQI Flags are bit packed byte variables. The byte column identifies the byte number(s) the PQI is stored in and the Bit column lists the bit(s) the flag encompasses within the byte(s). The name of the each flag is included, along with possible values.

### 3.4.3.4 Metadata

The metadata produced by the ABI-SO<sub>2</sub> are described in Table 10.

| Metadata Output  |
|--|
| Fraction of pixels that meet “Beta Object” membership criteria |
| Fraction of pixels that meet “BTD Object” membership criteria  |
| Fraction of pixels detected as SO <sub>2</sub>                 |
| Fraction of pixels with “low” SO <sub>2</sub> loading          |
| Fraction of pixels with “intermediate” SO <sub>2</sub> loading |
| Fraction of pixels with “heavy” SO <sub>2</sub> loading        |

**Table 10: A description of the SO<sub>2</sub> detection metadata.**

## 4 TEST DATA SETS AND OUTPUTS

### 4.1 Simulated/Proxy Input Data Sets

As described below, the data used to test the ABI-SO<sub>2</sub> consists of SEVIRI and MODIS observations. Both SEVIRI and MODIS have observed several SO<sub>2</sub> clouds. The rest of this section describes the proxy and validation data sets used in assessing the performance of the ABI-SO<sub>2</sub>.

#### 4.1.1 SEVIRI Data

SEVIRI provides 11 spectral channels with a spatial resolution of 3 km and provides spatial coverage of the full disk with a temporal resolution of 15 minutes. SEVIRI is a good proxy source for testing and developing the ABI-SO<sub>2</sub>. The SEVIRI to ABI channel mapping is shown in **Table 11**. Figure 8, shown below, is a full-disk SEVIRI image from 12 UTC on November 24, 2006. SEVIRI data are readily available from the University of Wisconsin Space Science and Engineering Center (SSEC) Data Center.

| SEVIRI Band Number | SEVIRI Wavelength Range ( $\mu\text{m}$ ) | SEVIRI Central Wavelength ( $\mu\text{m}$ ) | ABI Band Number | ABI Wavelength Range ( $\mu\text{m}$ ) | ABI Central Wavelength ( $\mu\text{m}$ ) |
|--------------------|---|---|-----------------|--|--|
| 5                  | 5.32 – 7.15                               | 6.20  | 8               | 5.70 – 6.60                            | 6.15                                     |
| 6                  | 6.85 – 7.85                               | 7.30  | 10              | 7.30 – 7.50                            | 7.40                                     |
| 7                  | 8.30 – 9.10                               | 8.70  | 11              | 8.30 – 8.70                            | 8.50                                     |
| 9                  | 9.80 – 11.80                              | 10.80                                       | 14              | 10.80 – 11.60                          | 11.20                                    |
| 10                 | 11.00 – 13.00                             | 12.00                                       | 15              | 11.80 – 12.80                          | 12.30                                    |

**Table 11:** The SEVIRI bands used to test the ABI SO<sub>2</sub> detection algorithm is shown relative to the corresponding ABI bands.



**Figure 8: SEVIRI RGB image from 12 UTC on November 24, 2006.**

#### 4.1.2 MODIS Data

MODIS provides 36 spectral channels with a spatial resolution of 1 km and provides global coverage in low Earth orbit. MODIS has observed many volcanic eruptions. The MODIS to ABI channel mapping is shown in *Table 12*. An example MODIS false color image is shown in *Figure 9*

| MODIS Band Number | MODIS Wavelength Range ( $\mu\text{m}$ ) | MODIS Central Wavelength ( $\mu\text{m}$ ) | ABI Band Number | ABI Wavelength Range ( $\mu\text{m}$ ) | ABI Central Wavelength ( $\mu\text{m}$ ) |
|-------------------|--|--|-----------------|--|--|
| 27                | 6.535 – 6.895                            | 6.715                                      | 8               | 5.70 – 6.60                            | 6.15                                     |
| 28                | 7.175 – 7.475                            | 7.325                                      | 10              | 7.30 – 7.50                            | 7.40                                     |
| 29                | 8.400 – 8.700                            | 8.550                                      | 11              | 8.30 – 8.70                            | 8.50                                     |
| 31                | 10.780 – 11.280                          | 11.03                                      | 14              | 10.80 – 11.60                          | 11.20                                    |
| 32                | 11.770 – 12.270                          | 12.02                                      | 15              | 11.80 – 12.80                          | 12.30                                    |

**Table 12:** The MODIS bands used to test the ABI volcanic ash algorithm is shown relative to the corresponding ABI bands.

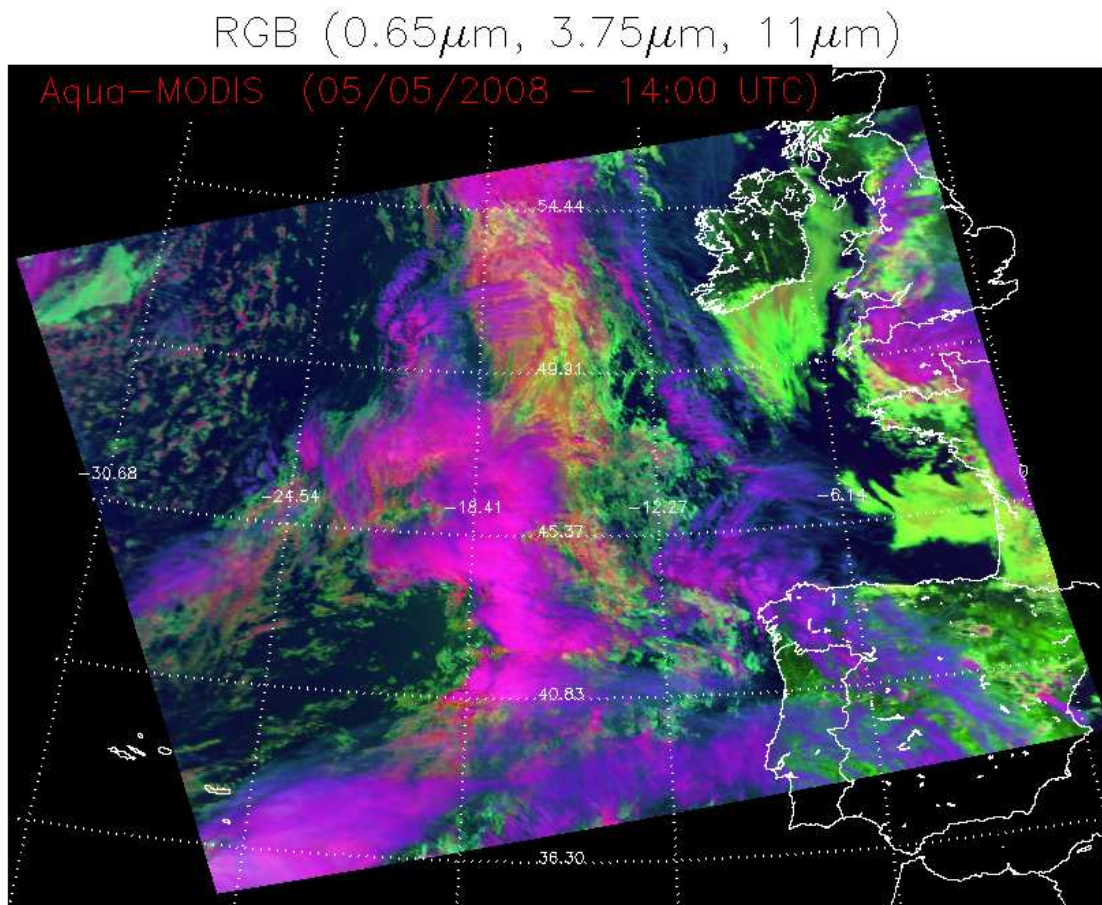


**Figure 9:** MODIS RGB image from 14 UTC on May 5, 2008.

### 4.1.3 OMI Data

With the launch of the Ozone Mapping Instrument (OMI) into the EOS A-train, the ability to monitor SO<sub>2</sub> on a global scale increased significantly. Currently, we are using OMI SO<sub>2</sub> loading retrievals to validate the ABI-SO<sub>2</sub>. OMI uses high spectral resolution ultra-violet (UV) measurements to retrieve the total column SO<sub>2</sub> loading, and is sensitive to very small loadings (< 1 DU). As such, OMI is much more sensitive to SO<sub>2</sub> than the ABI. An example OMI SO<sub>2</sub> product is shown in Figure 10.

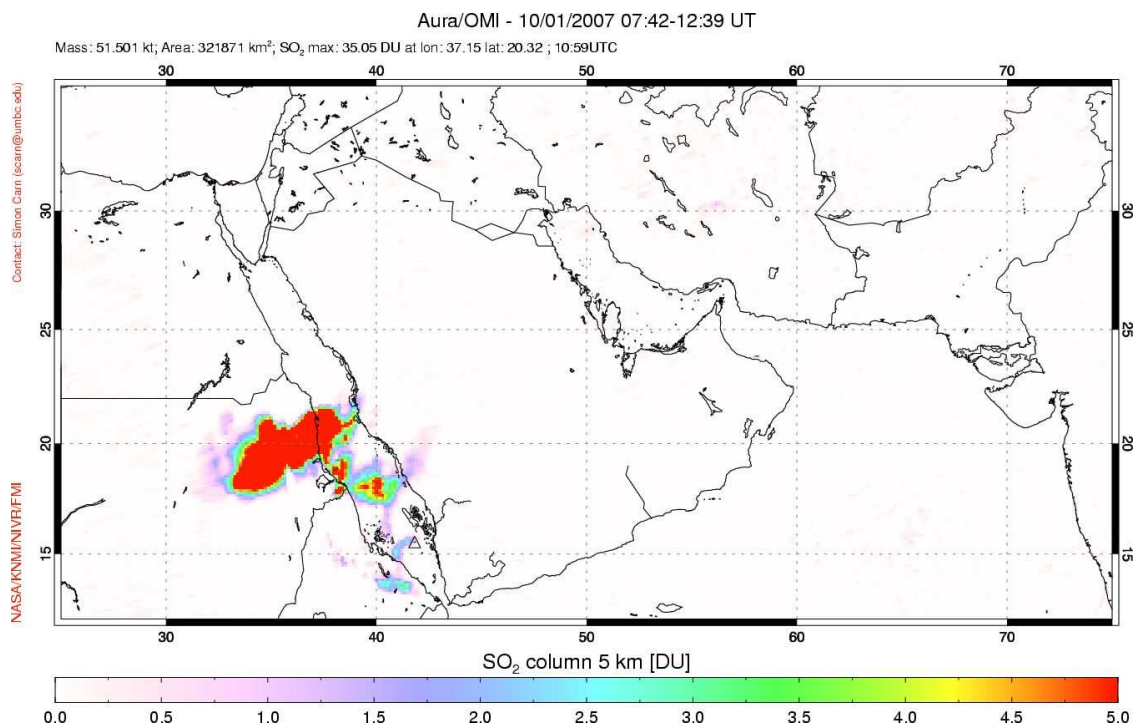


**Figure 10:** The OMI SO<sub>2</sub> loading product shows an SO<sub>2</sub> plume associated with an eruption of Jebel al-Tair in Yemen on October 1, 2007.

## 4.2 Output from Simulated/Proxy Inputs Data Sets

The ABI-SO<sub>2</sub> was tested on many SEVIRI and MODIS scenes. Example SEVIRI results are shown in Figure 11 for an eruption of Nyamuragira and example MODIS results are shown in Figure 12 for an eruption of Kasatochi. The SEVIRI full disk results show that the false alarm rate is very low, as the actual SO<sub>2</sub> cloud is the only feature in the full disk that is flagged as SO<sub>2</sub>. The SO<sub>2</sub> clouds appear yellowish-green in the false color images,

and the SO<sub>2</sub> detection results for both SEVIRI and MODIS closely match the location of the SO<sub>2</sub> in the false color imagery.

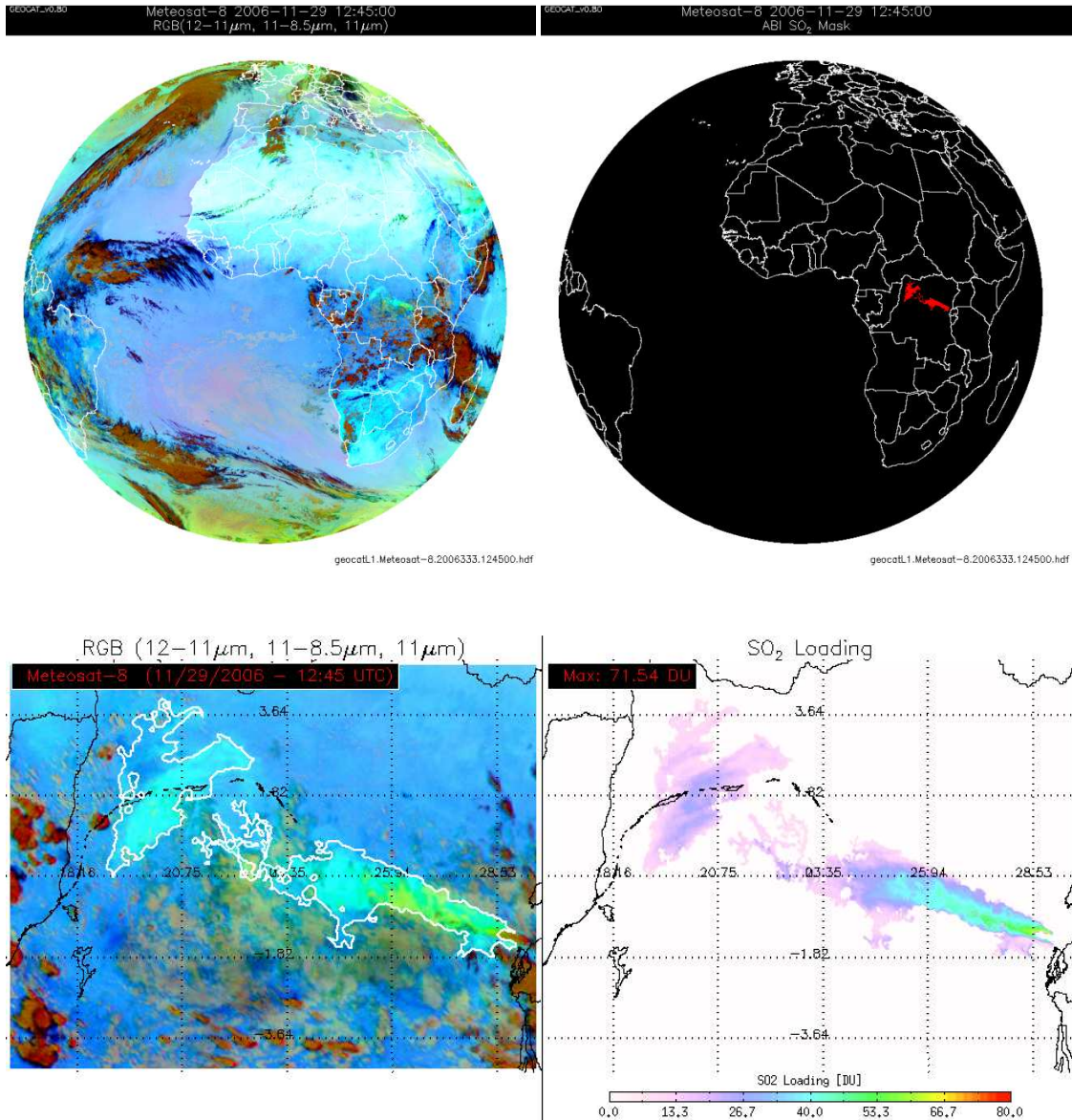


**Figure 11:** Example results from the ABI-SO<sub>2</sub> are shown for a Met-8 SEVIRI observed eruption of Nyamuragira in central Africa on November 29, 2006 at 12:45 UTC. The full disk results are shown in the top row (false color on left, SO<sub>2</sub> detection in red on the right). A zoomed in view is shown in the bottom row, including an estimate of the SO<sub>2</sub> loading, which is stored in the quality flags.

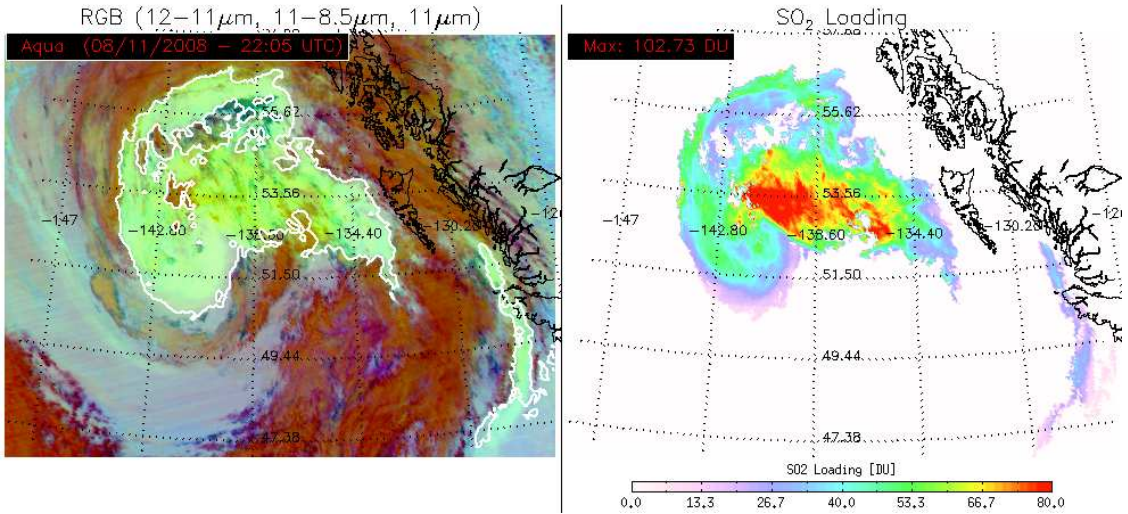


**Figure 12:** Example results from the ABI-SO<sub>2</sub> are shown for a *Aqua*-MODIS observed eruption of Kasatochi in the Aleutian Islands on August 11, 2008 at 22:05 UTC. The SO<sub>2</sub> detection results are overlaid as white contours on a false color image on the left panel and the estimated SO<sub>2</sub> loading is shown in the right panel.

#### 4.2.1 Precisions and Accuracy Estimates

To estimate the precision and accuracy of the ABI-SO<sub>2</sub>, we will primarily compare the ABI results to the OMI (Ozone Monitoring Instrument) SO<sub>2</sub> products. OMI, which is on the *Aura* spacecraft, is a UV spectrometer that can detect SO<sub>2</sub> loading of less than 1 DU, hence it is far more sensitive to the presence of SO<sub>2</sub> than the ABI. Given the sensitivity of the OMI, the ABI-SO<sub>2</sub> probability of detection and probability of false alarm can readily be diagnosed by comparing to the official OMI SO<sub>2</sub> product. Another advantage of using OMI is that the total column SO<sub>2</sub> amount is retrieved. Thus, we can characterize the ABI-SO<sub>2</sub> as a function of OMI SO<sub>2</sub> loading. One disadvantage of the OMI data is that the measurements are only valid during the day, but the ABI-SO<sub>2</sub> only utilizes infrared channels (e.g. it works the same day and night) so this should not be an issue.

##### 4.2.1.1 OMI Analysis

According to the F&PS, the ABI-SO<sub>2</sub> must detect SO<sub>2</sub> with a (Peirce-Hanssen-Kuipers) skill score of at least 0.70 when 10 DU or more of SO<sub>2</sub> is present. In order to determine the probability of false alarm and the probability of detection, and hence calculate a skill score, we co-located OMI SO<sub>2</sub> retrievals and the ABI SO<sub>2</sub> detection results from *Aqua* MODIS in time and space. The OMI flies aboard the *Aura* spacecraft, which is in a very similar orbit as *Aqua*, so the time difference between the measurements is very small. A total of 35 MODIS scenes (270,000 MODIS pixel match-ups) containing SO<sub>2</sub> clouds were used in the validation analysis. Prior to comparing the OMI and ABI-SO<sub>2</sub> results,

the OMI quality flags were used to filter out low quality OMI retrievals. Finally, the validation results were computed as a function of the OMI derived SO<sub>2</sub> loading. Those results are shown in the next section

#### 4.2.2 Error Budget

Figure 13 shows the ABI SO<sub>2</sub> detection skill score as a function of the OMI SO<sub>2</sub> loading. Over 270,000 data points went into this analysis. The results indicate that the ABI-SO<sub>2</sub> achieves the required skill score of 0.70 when 11.5 DU or more of SO<sub>2</sub> is present. This is very close (within the OMI loading error bar) to the required 0.70 skill score when 10 DU or more of SO<sub>2</sub> is present. Prior to the 100% delivery of the ABI-SO<sub>2</sub>, several incremental improvements will be made, which should increase the skill score.

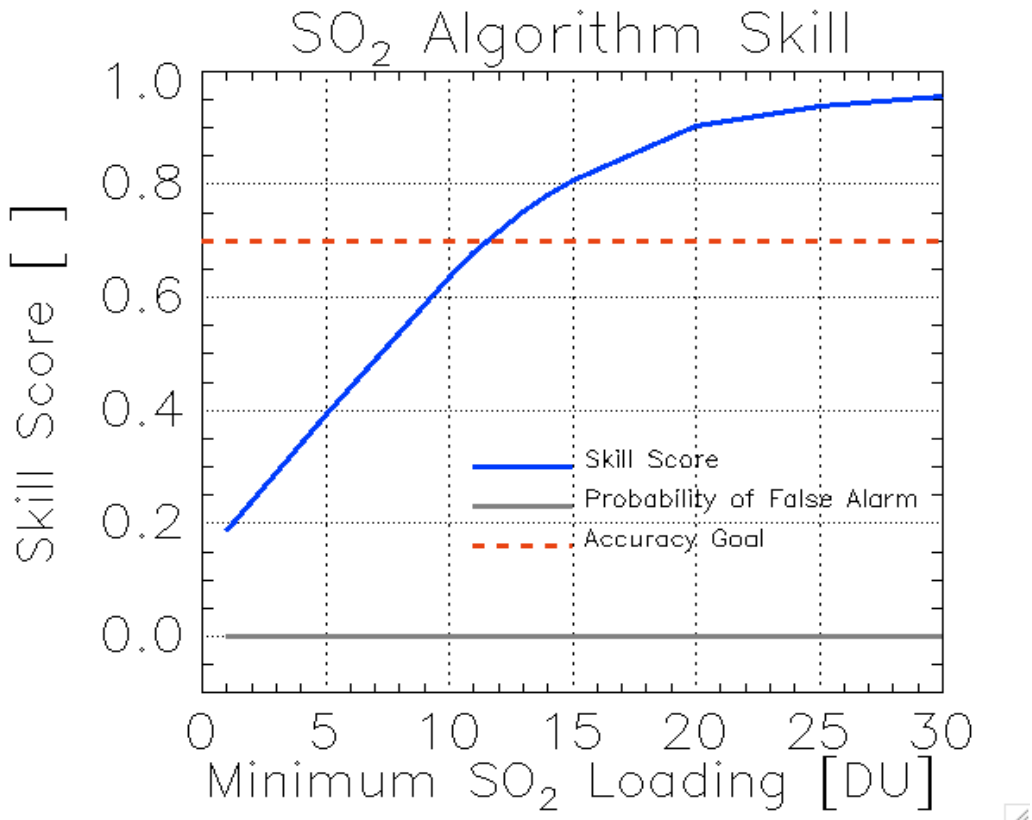


**Figure 13:** The ABI SO<sub>2</sub> detection skill score is shown as a function of the OMI SO<sub>2</sub> loading in blue. The false alarm rate is shown in gray, and the required SO<sub>2</sub> detection skill score is shown in dashed red. The required detection skill score only applies to SO<sub>2</sub> loadings of 10 DU or greater. This analysis was constructed using over 270,000 data points.

## **5 PRACTICAL CONSIDERATIONS**

### **5.1 Numerical Computation Considerations**

Prior to converting cloud emissivity to optical depth, the cloud emissivity must be checked to ensure that it is greater than 0.0 and less than 1.0 to prevent an illegal natural logarithm operation.

### **5.2 Programming and Procedural Considerations**

The ABI-SO<sub>2</sub> makes heavy use of clear-sky radiative transfer calculations. Our current system computes the clear-sky atmospheric transmittances at low spatial resolution and with enough angular resolution to capture sub-grid variation path-length changes. This step is critical, as performing clear-sky atmospheric transmittance calculations for each pixel requires extensive memory and CPU time, but does not produce significantly better scientific results. The AIADD Document describes this procedure in detail.

NWP data is heavily utilized in the ABI SO<sub>2</sub> detection algorithm. The algorithm can tolerate the use NWP data for forecasts ranging from 0 to 24 hours.

The ABI SO<sub>2</sub> detection algorithm can provide usable results out to a viewing angle of 80 degrees (the F&PS minimum requirement is 70 degrees).

### **5.3 Quality Assessment and Diagnostics**

It is recommended that clear sky radiance biases are regularly monitored and that the validation exercises described earlier are applied routinely. Further, algorithm performance issues are best diagnosed by examining the  $\beta$ -ratios used to detect microphysical anomalies.

### **5.4 Exception Handling**

Prior to use, the ABI-SO<sub>2</sub> checks to make sure that each channel falls within the expected measurement range and that valid clear sky radiance and transmittance profiles are available for each channel. The ABI-SO<sub>2</sub> is only applied to a given pixel if all channels used in the algorithm contain valid data (according to the L1b calibration flags); otherwise the algorithm output is flagged as missing. The science of the ABI-SO<sub>2</sub> algorithm does not allow for a graceful degradation of the products at this time. The algorithm, however, can tolerate the use NWP data for forecasts ranging from 0 to 24 hours.

### **5.5 Algorithm Validation**

We recommend that manual analysis along with the OMI analysis shown in Section 4.2.2 be adopted as the main validation tool. Since hyperspectral UV measurements, like those from OMI, are needed to monitor the stratospheric ozone layer, these measurements are a very high priority in the international community and will be available for the foreseeable future.

## 6 ASSUMPTIONS AND LIMITATIONS

The following sections describe the current limitations and assumptions in the current version of the ABI-SO2

### 6.1 Performance

The following assumptions have been made in developing and estimating the performance of the ABI-SO2. The following lists contain the current assumptions and proposed mitigation strategies.

1. NWP data of comparable or superior quality to the current 6 hourly GFS forecasts are available. (Mitigation: Use longer-range GFS forecasts or switch to another NWP source – e.g. ECMWF).
2. Top-of-atmosphere clear sky radiances are available for each pixel and 101 level profiles of clear sky atmospheric transmittance and radiance are available at the NWP data horizontal resolution. (Mitigation: Use reduced spatial resolution top-of-atmosphere clear sky radiances. The profiles of transmittance and radiance must be present at, at least, the NWP spatial resolution and 101 vertical levels).
3. All of the static ancillary data are available at the pixel level. (Mitigation: Reduce the spatial resolution of the surface type, land mask and or coast mask).
4. The processing system allows for processing of multiple scan lines at once for application of important spatial analysis techniques. (Mitigation: No mitigation is possible).

In addition, the clear sky radiance calculations are prone to large errors, especially near coastlines, in mountainous regions, snow/ice field edges, and atmospheric frontal zones, where the NWP surface temperature and atmospheric profiles are less accurate. The impact of these errors on the SO<sub>2</sub> detection depends on the cloud optical depth. For optically thick clouds (infrared optical depth of about 1.0 or greater), these errors have a small impact on the calculation of the effective absorption optical depth ratios since the difference between the observed and black cloud radiance approaches zero as the cloud optical depth increases. This is not the case for optically thin clouds, where inaccurate

NWP data can have serious impacts. The ABI-SO<sub>2</sub> utilizes the Local Radiative Center (LRC) (see Section 3.4.1.4 for details) concept to minimize these impacts, but improvements in NWP fields should lead to additional improvements in the ABI-SO<sub>2</sub>.

## 6.2 Assumed Sensor Performance

We assume the sensor will meet its current specifications. However, the ABI-SO<sub>2</sub> will be dependent on the following instrumental characteristics.

- Unknown spectral shifts in some channels will cause biases in the clear-sky RTM calculations that may impact the performance of the ABI-SO<sub>2</sub>. Clear sky radiance biases need to be monitored throughout ABI's lifetime.

## 6.3 Pre-Planned Product Improvements

We expect in the coming years to focus on the following improvements.

### 6.3.1 Incorporation of second water vapor channel

The 7.0- $\mu\text{m}$  water vapor channel, which is not very sensitive to SO<sub>2</sub>, can be compared to the 7.4- $\mu\text{m}$  water vapor channel, which is sensitive to SO<sub>2</sub>. This comparison may result in improvements since both channels have somewhat similar weighting functions.

## 7 REFERENCES

- Cox, S. K., 1976: Observations of Cloud Infrared Effective Emissivity. *J.Atmos.Sci.*, **33**, 287-289.
- Doutriaux-Boucher, M. and P. Dubuisson, 2008: Detection of volcanic SO<sub>2</sub> by spaceborne infrared radiometers. *Atmospheric Research*, **92**, 69-79.
- Giraud, V., J. C. Buriez, Y. Fouquart, F. Parol, and G. Seze, 1997: Large-scale analysis of cirrus clouds from AVHRR data: Assessment of both a microphysical index and the cloud-top temperature. *J.Appl.Meteorol.*, **36**, 664-675.
- Heidinger, A. K. and M. J. Pavolonis, 2009: Nearly 30 years of gazing at cirrus clouds through a split-window. Part I: Methodology. *J.Appl.Meteorol. and Climatology*, **48(6)**, 110-1116.
- Inoue, T., 1987: A Cloud Type Classification with Noaa 7 Split-Window Measurements. *J.Geophys.Res.-Atmos.*, **92**, 3991-4000.
- Parol, F., J. C. Buriez, G. Brogniez, and Y. Fouquart, 1991: Information-Content of Avhrr Channels 4 and 5 with Respect to the Effective Radius of Cirrus Cloud Particles. *J.Appl.Meteorol.*, **30**, 973-984.
- Pavolonis, M. J., 2010a: Advances in extracting cloud composition information from spaceborne infrared radiances: A robust alternative to brightness temperatures. Part I: Theory. *J. Applied Meteorology and Climatology*, In Press (available online).
- Pavolonis, M. J., 2010b: Advances in extracting cloud composition information from spaceborne infrared radiances: A robust alternative to brightness temperatures. Part II: Proof of concept. To be submitted to the *J. Applied Meteorology and Climatology*.
- Prata, A. J., W. I. Rose, S. Self, and D. M. O'Brien, 2003: Global, long-term sulphur dioxide measurements from TOVS data: A new tool for studying explosive volcanism and climate, in *Volcanism and the Earth's Atmosphere*, *Geophys. Monogr. Ser.*, vol. 139, edited by A. Robock and C. Oppenheimer, pp. 75-92, AGU, Washington, D.C.
- Prata, A. J. and J. Kerkman, 2007: Simultaneous retrieval of volcanic ash and SO<sub>2</sub> using MSG-SEVIRI. *Geophys. Research Letters*, **34**, L05813, doi:10.1029/2006GL028691.
- Seemann, S. W., E. E. Borbas, R. O. Knuteson, G. R. Stephenson, and H. Huang, 2008: Development of a global infrared land surface emissivity database for application to clear sky sounding retrievals from multispectral satellite radiance measurements. *J.Appl.Meteorol.Climatol.*, **47**, 108-123, doi:10.1175/2007JAMC1590.1.

Strow, L. L., S. E. Hannon, S. De Souza-Machado, H. E. Motteler, and D. Tobin, 2003: An overview of the AIRS radiative transfer model. *IEEE Trans.Geosci.Remote Sens.*, **41**, 303-313, doi:10.1109/TGRS.2002.808244 ER.

Turner, D. D., 2005: Arctic mixed-phase cloud properties from AERI lidar observations: Algorithm and results from SHEBA. *J.Appl.Meteorol.*, **44**, 427-444.

Van de Hulst, H. C., 1980: *Multiple Light Scattering, Tables, Formulas, and Applications*. Vol. 2. Academic Press, 739 pp.

Wielicki, B. A. and R. M. Welch, 1986: Cumulus cloud properties derived using Landsat Satellite Data. *J. Climate and Meteorology*, **25**(3), 261-276

Zhang, H., W. P. Menzel, 2002: Improvement in thin cirrus retrievals using an emissivity-adjusted CO<sub>2</sub> slicing algorithm. *J.Geophys.Res.-Atmos.*, **107**, 4327, doi:10.1029/2001JD001037.